Resource

Cell

CRISPR-Mediated Programmable 3D Genome Positioning and Nuclear Organization

Graphical Abstract

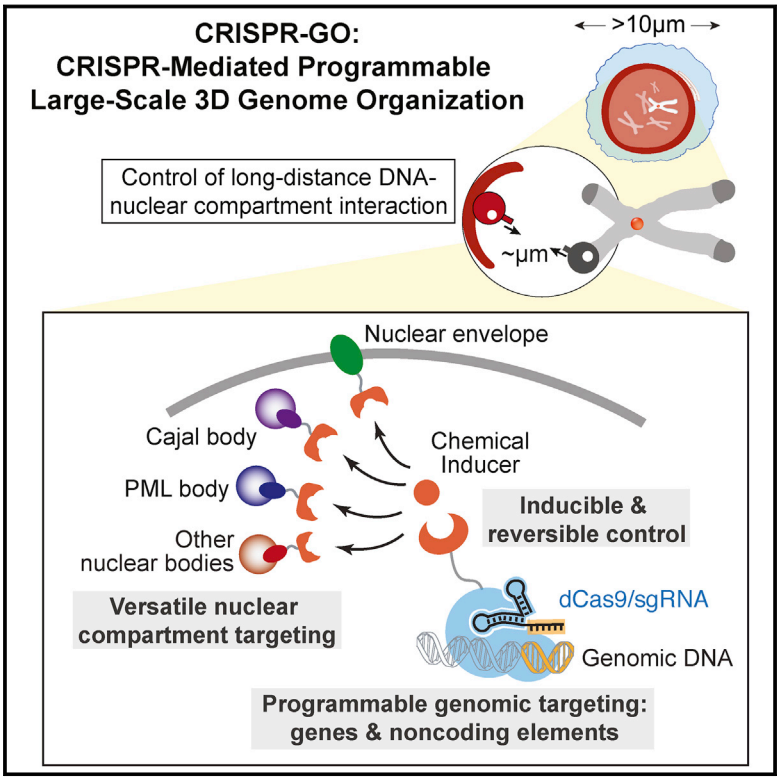

Authors

Haifeng Wang, Xiaoshu Xu, Cindy M. Nguyen, ..., Nathan H. Kipniss, Marie La Russa, Lei S. Qi

Correspondence

stanley.qi@stanford.edu

In Brief

An engineered CRISPR-based platform for inducible recruitment of specific genomic loci to distinct nuclear compartments reveals positional effects on gene expression and cellular function.

Highlights

- CRISPR-GO is a versatile system for targeting genome loci to nuclear compartments
- An inducible and reversible approach to study spatial genome organization
- CRISPR-GO mediates rapid and reversible *de novo* Cajal body (CB) formation
- CB-chromatin colocalization represses distal (30–600 kb) gene expression

Wang et al., 2018, Cell *175*, 1405–1417
November 15, 2018
https://doi.org/10.1016/j.cell.2018.09.013

CellPress

Resource

Cell

CRISPR-Mediated Programmable 3D Genome Positioning and Nuclear Organization

Haifeng Wang,[1] Xiaoshu Xu,[1] Cindy M. Nguyen,[1] Yanxia Liu,[1] Yuchen Gao,[1,2] Xueqiu Lin,[1] Timothy Daley,[1,3] Nathan H. Kipniss,[1] Marie La Russa,[1] and Lei S. Qi[1,4,5,6,*]

[1]Department of Bioengineering, Stanford University, Stanford, CA 94305, USA
[2]Cancer Biology Program, Stanford University, Stanford, CA 94305, USA
[3]Department of Statistics, Stanford University, Stanford, CA 94305, USA
[4]Department of Chemical and Systems Biology, Stanford University, Stanford, CA 94305, USA
[5]Stanford ChEM-H, Stanford University, Stanford, CA 94305, USA
[6]Lead Contact
*Correspondence: stanley.qi@stanford.edu
https://doi.org/10.1016/j.cell.2018.09.013

SUMMARY

Programmable control of spatial genome organization is a powerful approach for studying how nuclear structure affects gene regulation and cellular function. Here, we develop a versatile CRISPR-genome organization (CRISPR-GO) system that can efficiently control the spatial positioning of genomic loci relative to specific nuclear compartments, including the nuclear periphery, Cajal bodies, and promyelocytic leukemia (PML) bodies. CRISPR-GO is chemically inducible and reversible, enabling interrogation of real-time dynamics of chromatin interactions with nuclear compartments in living cells. Inducible repositioning of genomic loci to the nuclear periphery allows for dissection of mitosis-dependent and -independent relocalization events and also for interrogation of the relationship between gene position and gene expression. CRISPR-GO mediates rapid *de novo* formation of Cajal bodies at desired chromatin loci and causes significant repression of endogenous gene expression over long distances (30–600 kb). The CRISPR-GO system offers a programmable platform to investigate large-scale spatial genome organization and function.

INTRODUCTION

The 3-dimensional (3D) organization of the genome within the nucleus plays a central role in regulating gene expression and cellular function during development and in disease (Bickmore, 2013; Clowney et al., 2012; Yu and Ren, 2017). For example, genes that localize at the nuclear periphery exhibit low transcription, while those that localize to the nuclear interior often have higher activity (van Steensel and Belmont, 2017). During lymphocyte development, the immunoglobulin loci at the nuclear periphery in progenitor cells relocate to the nuclear interior in pro-B cells, a process that is synchronous with immunoglobulin activation and rearrangement (Kosak et al., 2002). Similarly, the gene locus of proneural transcription factor *Ascl1/Mash1* at the nuclear periphery of embryonic stem cells relocates to the nuclear interior of differentiated neurons (Williams et al., 2006).

Membraneless nuclear bodies are important for proper genome organization and cellular function (Mao et al., 2011). For example, Cajal bodies (CBs), which have been implicated in small nuclear RNA (snRNA) biogenesis, ribonucleoprotein assembly, and telomerase biogenesis, are essential for vertebrate embryogenesis and are also abundant in tumor cells and neurons (Gall, 2000). The promyelocytic leukemia (PML) nuclear bodies are also associated with tumorigenesis and antiviral infection (Reineke and Kao, 2009). However, the relationship between nuclear body/chromatin colocalization and gene expression remains poorly understood.

Our ability to study the causal relationship between 3D genome structure and gene expression is constrained by currently available methods. Microscopic imaging (e.g., fluorescent *in situ* hybridization, FISH) and chromosome conformation capture (3C)-based techniques have profiled changes in chromatin positioning and interactions during development and disease processes, providing valuable correlative information (Dekker et al., 2002; Langer-Safer et al., 1982; Yu and Ren, 2017). However, they often cannot establish causal links between genome organization and function.

Methods based on LacI-LacO interactions have been exploited to mediate targeted genomic reorganization. This technique utilizes an array of LacO repeats inserted into a genomic locus, which is recruited to the nuclear periphery using LacI fused to a nuclear membrane protein (Finlan et al., 2008; Kumaran and Spector, 2008; Reddy et al., 2008). Using this technique, repositioning genes to the nuclear periphery leads to gene repression (Finlan et al., 2008; Reddy et al., 2008). However, for this approach, creating a stable LacO repeat-containing cell line is a prerequisite, which involves multiple steps, including random insertion of a large LacO repeat array into the genome, screening for stable cell lines containing a single insertion locus, and characterization of the genomic insertion site. New tools are needed for programmable control of the spatial genome organization.

Prokaryotic class II CRISPR-Cas systems have been repurposed as a toolbox for gene editing, gene regulation, epigenome

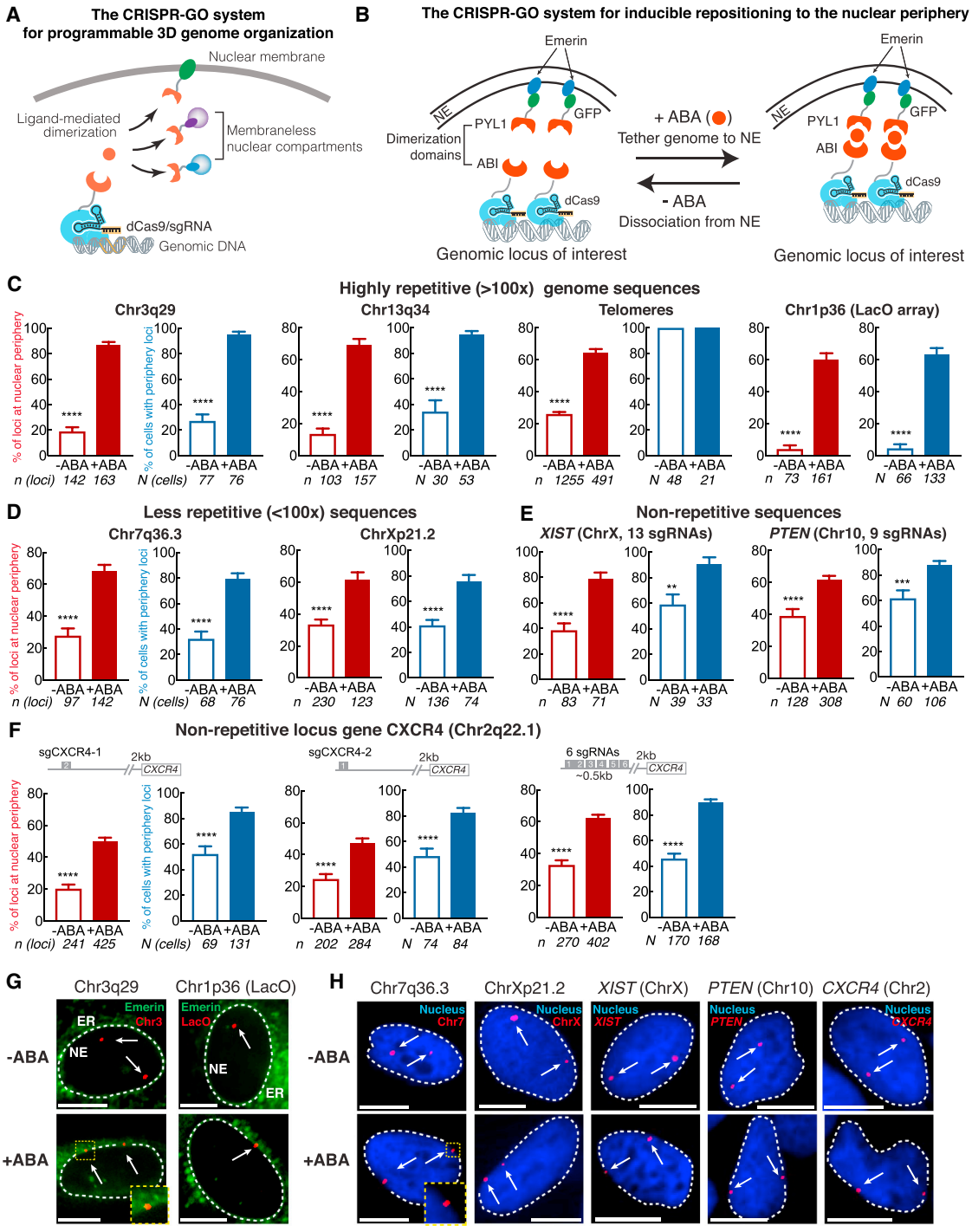

Figure 1. A Programmable CRISPR-GO System Efficiently Repositions Endogenous Genomic Loci to the Nuclear Periphery

(A) Schematic of a programmable and inducible CRISPR-GO system for targeting genomic loci to various nuclear compartments.

(B) Schematic of the abscisic acid (ABA)-inducible CRISPR-GO system to target genomic loci to the nuclear periphery via co-expression of ABI-dCas9 and PYL1-GFP-Emerin. NE: nuclear envelope.

(C) Quantification of CRISPR-GO genomic repositioning efficiency of highly repetitive genomic loci. Chr3, Chr13, and LacO loci are labeled using CRISPR-Cas9 imaging in living cells. Telomeres are labeled by a telomere marker, TRF1-mCherry. The NE is visualized by GFP-Emerin.

(D and E) Quantification of CRISPR-GO nuclear repositioning efficiency of less repetitive (D) or non-repetitive (E) endogenous genomic loci. Genomic loci are visualized by 3D-FISH and nuclei are stained by DAPI.

(F) Comparison of re-localization efficacy targeting *CXCR4* loci using single sgRNAs (sgCXCR4-1, left; sgCXCR4-2, middle) or 6 sgRNAs (right).

(legend continued on next page)

editing, chromatin looping, and live-cell genome imaging (Barrangou et al., 2007; Chen et al., 2013; Cong et al., 2013; Hilton et al., 2015; Jinek et al., 2012; Mali et al., 2013; Morgan et al., 2017; Qi et al., 2013). Nuclease-deactivated Cas (dCas) proteins coupled with transcriptional effectors allow regulation of gene expression adjacent to a single-guide RNA (sgRNA) target site (Gilbert et al., 2013; Qi et al., 2013). It remains unknown whether the CRISPR-Cas system can be used to mediate spatial genome organization and manipulate genomic interactions with nuclear compartments.

We developed a versatile system for programmable 3D genome organization, named CRISPR-genome organizer (CRISPR-GO), by coupling the CRISPR-dCas9 system with nuclear-compartment-specific proteins via ligand-mediated dimerization (Figure 1A). We showed that CRISPR-GO allowed for efficient, inducible, and dynamic repositioning of specific genomic loci to the nuclear periphery, Cajal bodies, and PML bodies. CRISPR-GO can be programmed to flexibly target different genomic sequences. By combining CRISPR-GO with live-cell CRISPR-Cas9 imaging, we were able to interrogate the real-time dynamics of chromatin interactions with nuclear compartments. Targeting genomic loci to the nuclear periphery or to Cajal bodies repressed proximal reporter gene expression. Importantly, colocalization of genomic loci with Cajal bodies repressed distal (30–600 kb) endogenous gene expression. The CRISPR-GO system offers a useful technology to study the relationship between macroscale (~μm) spatial genome organization and cellular function, distinct from previous uses of CRISPR for gene editing and local gene regulation.

RESULTS

Development of a Chemical-Inducible CRISPR-GO Platform for Target-Specific Genomic Repositioning

To implement an inducible CRISPR-mediated chromatin repositioning system, we first tested two chemical-inducible heterodimerization systems: an abscisic acid (ABA) inducible ABI/PYL1 system (Gao et al., 2016; Liang et al., 2011), and a Trimethoprim-Haloligand (TMP-Htag) inducible DHFR/HaloTag system (Ballister et al., 2014). For both systems, we fused the *Streptococcus pyogenes* dCas9 (D10A & H840A) protein to one heterodimer, and an inner nuclear envelope (NE) protein, Emerin to the cognate heterodimer (Figures 1B, S1A, and S1B). Emerin is inserted into the endoplasmic reticulum (ER) after synthesis, and then translocated to the NE through diffusion within the contiguous ER/NE membranes (Berk et al., 2013). We created U2OS human bone osteosarcoma cell lines that stably expressed each dimerization system. Addition of ABA caused efficient dimerization-induced re-localization of ABI-BFP-dCas9 protein from the nuclear interior to the NE and ER (Figures S1C and S1D), but the TMP-Htag inducible system showed no evident re-localization effects (data not shown). Therefore, we used the ABA-inducible ABI/PYL1 system for later experiments.

To test if the ABA-inducible CRISPR-GO system was able to alter the position of chromosomes, we introduced an sgRNA that targets a highly repetitive (>100x) endogenous region within Chromosome 3q29 (Chr3q29) (Ma et al., 2016) (Figures 1C and S2A, Table S1). To visualize the position of the targeted Chr3 locus, we added an independent CRISPR-Cas9 imaging component, a dCas9-HaloTag fusion protein, which binds to the JF549-HaloTag dye (Figure S1C) (Chen et al., 2013; Grimm et al., 2015). We confirmed that, in the absence of sgRNA, the localization of dCas9-HaloTag was unaffected by the ABA treatment (Figure S1D). The Chr3 sgRNA mediates both CRISPR-Cas9 imaging (via dCas9-HaloTag) and CRISPR-GO genomic re-localization (via ABI-dCas9) by targeting multiple repeats within the same Chr3 region. After 2 days of ABA treatment, the percentage of Chr3 loci that localized to the nuclear periphery increased from 19% to 87%, and the percentage of cells with periphery loci (i.e., cells showing at least one locus localized to the nuclear periphery) increased from 27% to 95% (Figures 1C, 1G, S3A, and S3B). CRISPR-GO is efficient in repositioning highly repetitive endogenous genomic loci in human cells.

The CRISPR-GO System Enables Efficient Repositioning of Repetitive Genomic Loci

We further tested repositioning other highly repetitive endogenous genomic loci to the nuclear periphery. By using an sgRNA that targets a repetitive region on chromosome 13q34 (Figure S2A, Table S1), the percentage of Chr13 loci at the nuclear periphery increased from 13% to 69%, and the percentage of cells with periphery loci increased from 34% to 94% (Figure 1C). Similarly, using a telomere-targeting sgRNA, the percentage of periphery-localized telomeres increased from 26% to 65% (Figure 1C, Videos S1 and S2).

We also targeted a LacO array located at chromosome 1p36 in a U2OS 2-6-3 reporter cell line (Figure S2A) (Kumaran and Spector, 2008). Based on CRISPR imaging, the percentage of periphery loci increased from 4% to 60%, and the percentage of cells with periphery loci increased from 4.5% to 65% after ABA treatment (Figures 1C and 1G), which was also confirmed by FISH (Figure S3C).

Next, we utilized 3D-FISH analysis to test the efficiency of the CRISPR-GO system to reposition less repetitive (<100 repeats) sequences. We chose to target a genomic region on Chr7q36.3 containing ~71 sgRNA-targetable repeats and a region on ChrXp21.2 containing ~15 repeats (Figure S2B). After ABA treatment, the percentage of periphery-localized loci increased from 28% to 68% for Chr7 and from 33% to 62% for ChrX. The percentage of cells with periphery loci increased from 32% to 79%

For (C)–(F), red: percentage of genomic loci at the nuclear periphery, n = total loci analyzed; blue: percentage of cells containing at least one nuclear periphery-localized locus, N = total cells analyzed. Data are represented as mean ± SEM. ** $p < 0.01$, *** $p < 0.001$, **** $p < 0.0001$. Positions of targeted loci are shown in Figure S2 and Tables S1 and S2.

(G and H) Representative microscopic images comparing the localization of targeted genomic loci (red, arrows) labeled by CRISPR-Cas9 imaging (G) or 3D-FISH (H) in ± ABA conditions. (G) PYL1-GFP-Emerin (green) localized to the NE and endoplasmic reticulum (ER). (H) Nuclei labeled by DAPI (blue). The nuclear periphery is outlined by dotted white lines except for regions next to peripheral genomic loci. Insets show enlarged images of peripheral genomic loci. Scale bars, 10μm. See also Figure S1, S2, and S3 and Tables S1 and S2.

for Chr7 and from 41% to 76% for ChrX (Figures 1D and 1H). When using a non-targeting sgRNA as a control, the percentages of periphery loci remained unchanged after ABA treatment (Figure S3D). These results suggest that our CRISPR-GO system is efficient in repositioning highly repetitive and less repetitive sequences to the nuclear periphery.

The CRISPR-GO System Enables Efficient Repositioning of Non-repetitive Genomic Loci

While repetitive sequences are abundantly present in the human genome, we asked if the CRISPR-GO system also enabled repositioning of non-repetitive genomic loci. We first chose to target the non-repetitive *XIST* gene located at ChrXq13.2 and designed 13 sgRNAs spanning the *XIST* genomic region (Figure S2C, Table S2). With ABA treatment, the percentage of periphery-localized *XIST* loci increased from 39% to 79%, and the percentage of cells with periphery loci increased from 59% to 90% (Figures 1E and 1H). By using a pool of 9 sgRNAs targeting regions adjacent to and within the *PTEN* gene on Chr10 (Figure S2C, Table S2), the CRISPR-GO system increased the percentage of periphery localized *PTEN* loci from 39% to 61% and the percentage of cells from 62% to 88% (Figures 1E and 1H).

We also tested whether a single sgRNA targeting a non-repetitive region was sufficient to re-reposition a genomic locus. Using a single sgRNA targeting the *CXCR4* locus at Chr2, the percentage of periphery localized *CXCR4* loci increased from 20% to 50% (sgCXCR4-1) or from 25% to 47% (sgCXCR4-2). The percentage of cells with periphery loci increased from 52% to 85% (sgCXCR4-1) or from 49% to 82% (sgCXCR4-2) (Figures 1F and S2C, Table S2). When using a pool of 6 sgRNAs, the CRISPR-GO system increased the percentage of periphery *CXCR4* loci from 32% to 62%, and the percentage of cells from 46% to 90%, respectively (Figures 1F and 1H). In the non-targeting sgRNA control group, the percentage of periphery *CXCR4* loci remained unchanged after ABA treatment (Figure S3D). These results together suggested that the CRISPR-GO system can mediate efficient relocalization of non-repetitive loci to the nuclear periphery.

CRISPR-GO-Mediated Genomic Repositioning Is Chemically Inducible and Reversible

One advantage of the CRISPR-GO system is its ability to easily switch on or off genomic re-positioning by adding or removing a chemical inducer. We performed chemical induction and removal experiments to study the system's dynamics and reversibility (Figure 2A). ABA-induced genomic re-localization occurred relatively quickly, as the percentage of periphery Chr3 loci increased from 19% ($n = 142$) to 75% ($n = 93$, $p < 0.0001$) within 16 hr of ABA addition and reached 91% ($n = 160$) after 72 hr. After ABA removal, the percentage of periphery Chr3 loci decreased from 82% ($n = 163$) to 45% ($n = 84$, $p < 0.0001$) after 24 hr and further decreased to 27% ($n = 146$) and 26% ($n = 159$) after 48 hr and 72 hr, respectively. After 48 hr of ABA removal, the percentage of periphery Chr3 was indistinguishable from an untreated sample (25%, $n = 106$, $p = 0.77$). These results suggest that nuclear repositioning mediated by the CRISPR-GO system can be easily switched on and off by adding or removing the ABA chemical inducer.

CRISPR-GO System-Mediated Nuclear Periphery Repositioning Occurs via Mitosis-Dependent and -Independent Mechanisms

Previous work using the LacO-LacI system found that tethering of the LacO locus to the nuclear periphery is mitosis dependent (Kumaran and Spector, 2008). We re-visited this question using the CRISPR-GO system to target the endogenous Chr3 locus. CRISPR-GO cells containing Chr3-targeting sgRNAs were synchronized and arrested at S phase by Hydroxyurea (HU) treatment and then treated with ABA (Figure 2B). Interestingly, after 24 hr of ABA treatment, the percentage of periphery Chr3 loci increased from 17% ($n = 175$) to 33% ($n = 177$, $p = 0.0008$) in S-phase arrested cells, which was significantly lower than in unsynchronized cells (75%, $n = 251$, $p = 0.0001$). After 48 hr of ABA treatment, the percentage of periphery Chr3 loci increased to 54% ($n = 177$, $p < 0.0001$) in S-phase arrested cells, which was also lower than in unsynchronized cells (83%, $n = 178$, $p < 0.0001$). Thus, in S-phase arrested cells, nuclear periphery repositioning was still observed but to a lesser extent than cells that underwent mitosis, suggesting that the repositioning may happen via both mitosis-dependent and -independent mechanisms.

To our knowledge, mitosis-independent periphery repositioning has not yet been reported. Using live-cell CRISPR-Cas9 imaging, we detected the dynamic process of endogenous Chr3 loci being tethered to the nuclear periphery during interphase (Figures 2C, 2D, and S3E). In an example cell, a Chr3 locus (red, arrow) started off separate from the nuclear periphery (green, GFP-Emerin) during the first 4 hr of recording, became tethered to the nuclear periphery at 4.5 hr, and stayed tethered for the remaining 8 hr of recording even while the nucleus underwent a rotation between 10 hr and 12 hr. Regardless of the stable organization of chromatin structure during interphase, these results indicated that a genomic locus located close to the nuclear periphery can be tethered to the nuclear periphery in a mitosis-independent manner.

Real-Time Live-Cell Imaging Reveals that Tethering at the Nuclear Periphery Suppresses Movements of Endogenous Genomic Loci

We studied the short-time movement kinetics of genomic loci by characterizing the displacement between the consecutive movement steps of each locus in a 2-dimensional space (Figure 2E). Periphery localized Chr3 loci exhibited more confined movement, confirming the physical tethering of these loci to the nuclear envelope. The periphery-tethered Chr3 loci presented a much lower step distance of 0.04 ± 0.03 μm than untethered loci (0.11 ± 0.07 μm, Figure 2F), which were well approximated by distinct gamma distributions (Figure 2G). These results suggest that nuclear periphery tethering mediated by the CRISPR-GO system suppresses the mobility of endogenous genomic loci.

The CRISPR-GO System Can Trigger Colocalization of Genomic Loci with Membraneless Nuclear Bodies Including Cajal Bodies and PML Bodies

We next tested whether the CRISPR-GO system can mediate colocalization of chromatin loci with membraneless nuclear

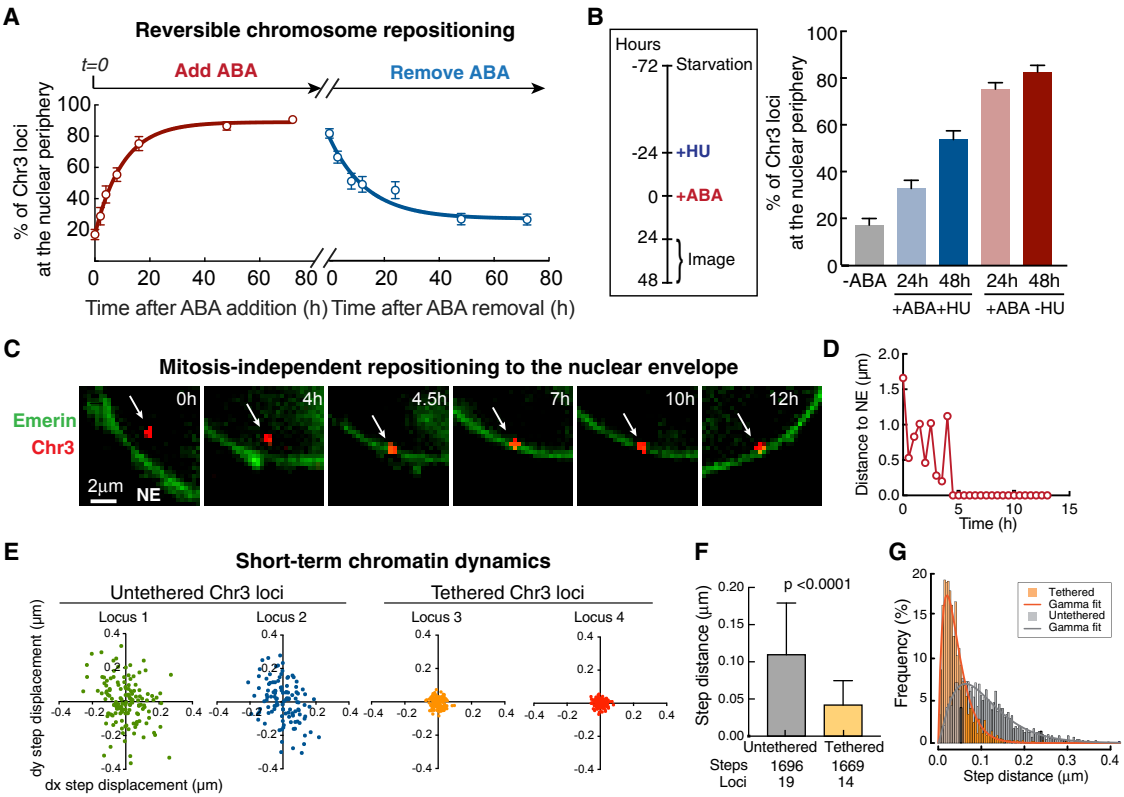

Figure 2. CRISPR-GO Enables Reversible Control of Chromosome Repositioning and Study of the Real-Time Dynamics of the Process

(A) Time course of the inducible and reversible repositioning of endogenous Chr3 loci, mediated by addition or removal of ABA. The y axis shows the percentage of peripherally localized Chr3 loci. The x axis shows the time in hr from ABA addition or removal.

(B) Comparison of the genomic repositioning efficacy in S-phase arrested cells (+ABA, +HU) and control cells (+ABA, -HU) at different time points after ABA addition. The box (left) shows an outline of the time-course experiment. HU, hydroxyurea.

For (A) and (B), data are represented as mean ± SEM.

(C) Representative microscopic images showing mitosis-independent repositioning of Chr3 loci (red, arrow) to the nuclear envelope (green, NE). Nuclear periphery tethering occurs at 4.5h. Images here are insets in Figure S3E. Scale bar, 2μm.

(D) A diagram showing the distances between the genomic locus in (C) (arrow) and nearest nuclear envelope at different time points. Images were taken every 30 mins.

(E) Scatterplots of step displacement (dx, dy) of untethered (1&2) and tethered (3&4) Chr3 loci. $dx^t = (x^t - x^{t-1})$ and $dy^t = (y^t - y^{t-1})$, where (x^t, y^t) is the coordinate of a locus at time t. Movements were tracked every 4 s for 6 min.

(F) Comparison of average step distance of untethered (1696 steps of 19 loci) and tethered (1669 steps of 14 loci) Chr3 loci. Data are represented as mean ± SD.

(G) Fitting of the step distances of untethered and tethered Chr3 loci using gamma distribution. See also Figure S3.

bodies. Nuclear bodies are proposed to assemble through liquid-liquid phase separation, which is driven by multivalent RNA-protein interactions (Zhu and Brangwynne, 2015).

To recruit genomic loci to Cajal bodies (CBs), we designed a CB-targeting CRISPR-GO system by fusing PYL1 with Coilin, a marker of Cajal bodies (Figure 3A). We tested the recruitment efficiency targeting the LacO loci in U2OS 2-6-3 cells (Kumaran and Spector, 2008). After 2 days of ABA treatment, the percentage of LacO loci that colocalized with GFP-Coilin-labeled CBs increased from 9% to 64%, and the percentage of cells that contained at least one CB colocalized with a LacO locus increased from 10% to 65% (Figures 3B and 3C, $p < 0.0001$). Combined immunostaining with FISH showed that other CB components (SMN, Fibrillarin, and Gemin2) also colocalized with LacO loci after 20 hr of ABA treatment (Figure 3D), confirming CRISPR-GO-mediated colocalization of the targeted genomic loci with CBs.

To target endogenous genomic loci to CBs, we introduced the Chr3q29-targeting sgRNA into U2OS cells expressing the CB-targeting CRISPR-GO system. After 24 hr of ABA treatment, the percentage of Chr3 loci that colocalized with CBs increased from 2% to 94% ($p < 0.0001$), and the percentage of cells containing at least one CB colocalized with a Chr3 locus increased from 6% to 96% ($p < 0.0001$) (Figures 3E and 3F).

We also tested whether CRISPR-GO could mediate colocalization of endogenous chromatin loci with PML nuclear bodies. To do this, we designed a PML body-targeting CRISPR-GO system by fusing PYL1 with PML, the scaffold protein of PML bodies, and introduced the Chr3-targeting sgRNA into cells expressing both PYL1-GFP-PML and ABI-dCas9 (Figures 3G and 3H). Interestingly, a high percentage (52.6%) of Chr3 loci colocalized with the PML bodies without ABA treatment, which suggests natural Chr3q29-PML body colocalization (Figures 3H and 3I). After ABA treatment, the percentage of Chr3 loci that colocalized with PML

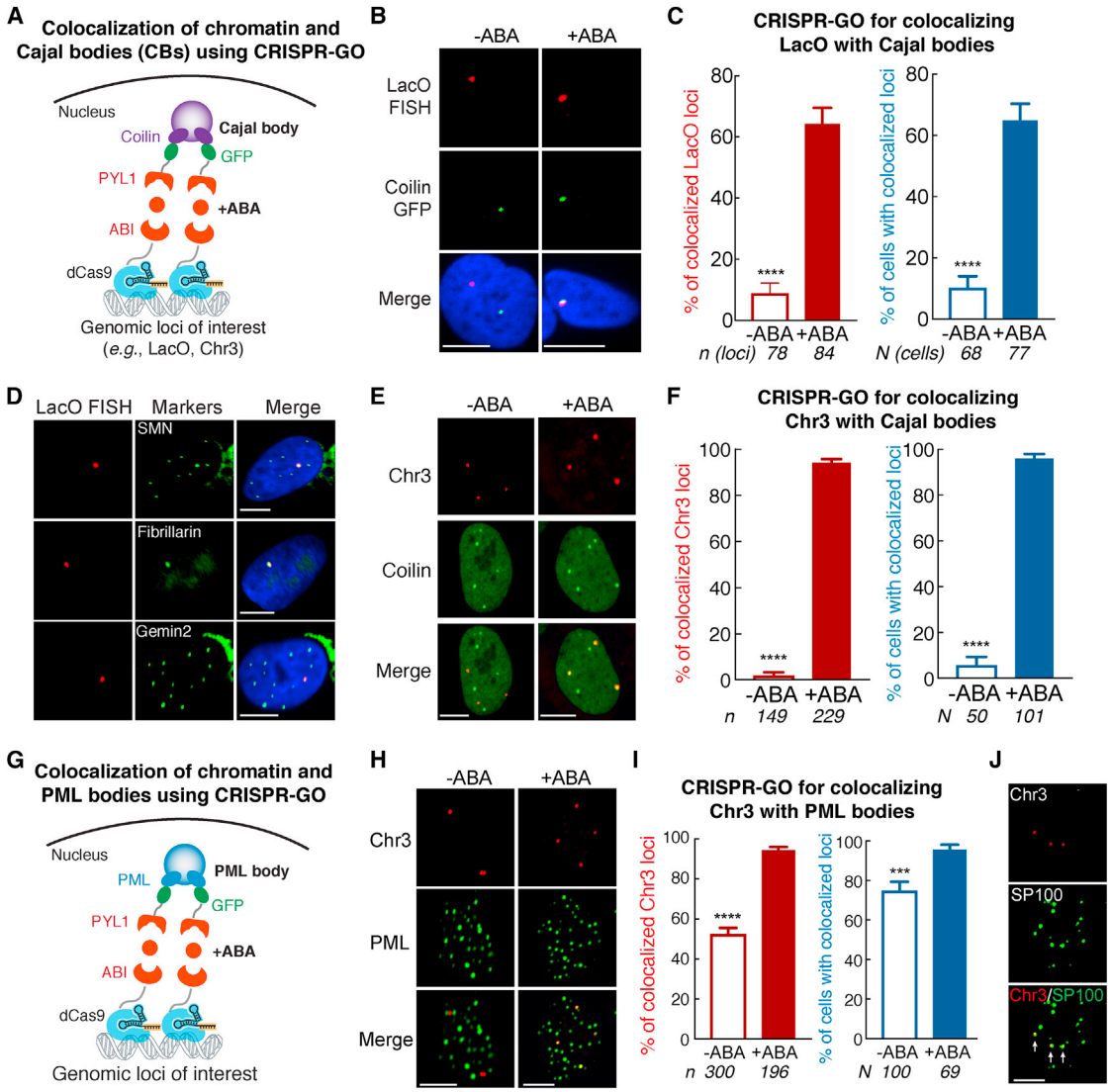

Figure 3. CRISPR-GO Enables Colocalization of Targeted Chromatin Loci with Nuclear Bodies, Including Cajal Bodies and PML Bodies

(A) Schematic of the ABA-inducible CRISPR-GO system for targeting genomic loci to CBs through co-expression of ABI-dCas9 and PYL1-GFP-Coilin.

(B) Representative microscopic images showing colocalization of the targeted LacO loci (red, by FISH) and Coilin-GFP-labeled CBs (green) in −/+ ABA conditions.

(C) Quantification of CRISPR-GO CB tethering efficiency of LacO loci.

(D) Colocalization of other CB components (green, SMN, Fibrillarin, Gemin2, by immunostaining) with LacO loci (red, by FISH) using the CRISPR-GO system to target LacO loci to CBs.

(E) Representative microscopic images showing colocalization of targeted Chr3 loci (red, by CRISPR-Cas9 imaging) and Coilin-GFP labeled CBs (green) in −/+ ABA conditions.

(F) Quantification of CRISPR-GO CB-tethering efficiency of Chr3 loci.

(G) Schematic of the ABA-inducible CRISPR-GO system for targeting genomic loci to PML bodies through co-expression of ABI-dCas9 and PYL1-GFP-PML.

(H) Representative microscopic images showing colocalization of targeted Chr3 loci (red, by CRISPR-Cas9 imaging) and PML-GFP labeled PML bodies (green) in −/+ ABA conditions.

(I) Quantification of CRISPR-GO PML body tethering efficiency to the targeted Chr3 loci. For C, F&I, Red: the percentage of targeted loci that colocalize with CBs (C&F) or PML bodies (I), n = total loci analyzed; Blue: the percentage of cells containing at least one CB-colocalized (C&F) or PML body-colocalized (I) locus, N = total cells analyzed. *** indicates $p < 0.001$, **** indicates $p < 0.0001$. Data are represented as mean ± SEM.

(J) Colocalization of another PML body marker, SP100 (green, immunostaining), with Chr3 loci (red) after using CRISPR-GO to target Chr3 loci to PML bodies in +ABA condition. Scale bars, 10μm.

bodies increased to 94% ($p < 0.0001$), and the percentage of cells containing at least one PML body that colocalized with the Chr3 locus increased from 75% to 96% ($p = 0.0003$) (Figures 3H and 3I). We also confirmed Chr3-PML body colocalization after ABA treatment by immunostaining of SP100, another PML body marker (Figure 3J).

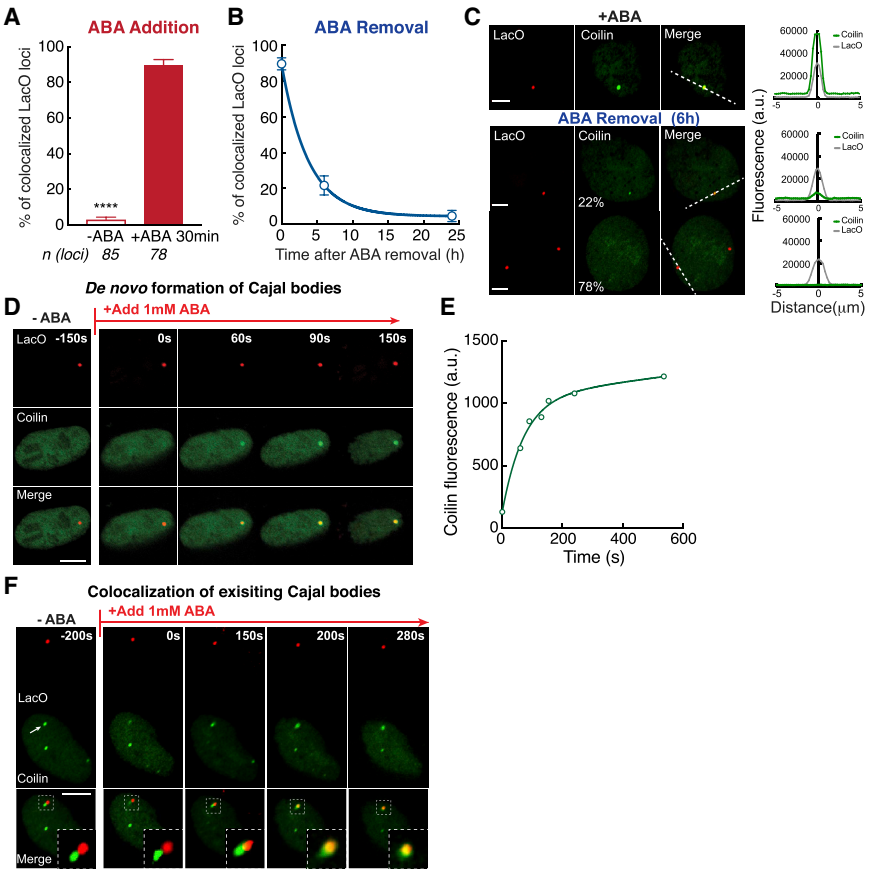

Figure 4. Dynamics of the Association and Dissociation of Chromatin and Cajal Bodies Mediated by CRISPR-GO

(A) Rapid, inducible chromatin-CBs association through addition of ABA. The y axis shows the percentage of CB-colocalized LacO loci. n = total loci analyzed. **** $p < 0.0001$.

(B) A diagram showing dynamics of chromatin-CBs disassociation after removal of ABA. The y axis shows the percentage of CB-colocalized LacO loci. x axis shows the time in hr from ABA removal. For (A) and (B), data are represented as mean ± SEM.

(C) Comparison of GFP-Coilin fluorescence (green) at targeted LacO loci (red) in cells treated with ABA (top) and 6 h after ABA removal (bottom two rows). Two representative cells are shown with dimmed CBs (middle) or cells in which CBs have disappeared (bottom). Linescan (right) measures the fluorescence intensity of GFP-Coilin (green) and LacO loci (gray) along the dotted lines (left).

(D) Real-time microscopic images showing rapid, *de novo* formation of a CB (Coilin, green) at the targeted LacO locus (red) mediated by CRISPR-GO. The chosen cell was initially imaged before ABA treatment (−150 s). ABA was added to the culture medium between −150 s and 0 s, and 0 s represents the first image taken of the same cell immediately after ABA addition.

(E) Quantification of the Coilin-GFP fluorescence intensity at the LacO locus shown in (D). The intensity before ABA addition was set to 0.

(F) Real-time microscopic images showing colocalization of an existing CB (Coilin, green, arrow) to an adjacent targeted LacO locus (red) mediated by CRISPR-GO. The chosen cell was imaged before ABA treatment (−200 s). ABA was added to the culture medium between −200 s and 0 s, and 0 s represents the first image taken immediately after ABA addition. Scale bars, 10μm.

CRISPR-GO Mediates Rapid, Inducible, and Reversible Association between Target Genomic Loci and Cajal Bodies

We again studied the dynamics and reversibility of CRISPR-GO-mediated chromatin colocalization with CBs. We observed rapid association of LacO loci with GFP-Coilin-marked CBs. Within 30 min after ABA addition, the percentage of LacO loci that colocalized with CBs increased from 2.6% to 89% ($p < 0.0001$) (Figure 4A).

In cells pretreated with ABA for 1 day, ABA removal led to dissociation of CBs from LacO loci. The percentage of CB-colocalized LacO loci decreased from 89% (n = 85) to 22% (n = 60, $p < 0.0001$) after 6 hr of ABA removal and further decreased to 4.6% (n = 45, $p < 0.0001$) after 24 hr (Figure 4B). At 6 hr after ABA removal, among the cell population (22%) that still possessed LacO-colocalized GFP-Coilin, the remaining GFP-Coilin intensity was much dimmer than that in cells undergoing sustained ABA treatment (Figure 4C), indicating a gradual disassembly of CBs.

CRISPR-GO Leads to both *De Novo* CB Formation and Repositioning of Existing CBs at Targeted Chromatin Loci

To further characterize the dynamics of CRISPR-GO-mediated association of CBs with targeted genomic loci, we performed time-lapse microscopy of individual cells. Previous reports using the LacO-LacI tethering system suggest that CBs form *de novo* at the targeted DNA site (Kaiser et al., 2008).

By using the CRISPR-GO system to target LacO loci to CBs, we observed rapid (within minutes) *de novo* CBs formation at the LacO locus in most analyzed cells after addition of ABA (Figure 4D). For example, a cell with no initial GFP-Coilin accumulation at the LacO locus (Figure 4D, −150 s) rapidly recruited GFP-Coilin to the LacO locus after ABA was added (between −150 s and 0 s, Figure 4D), causing *de novo* formation of CBs. The GFP-Coilin fluorescence intensity at the LacO loci approached saturation within 10 min after ABA addition (Figure 4E).

Interestingly, we also observed dynamic repositioning of the targeted chromatin locus with an existing CB when the two were initially close to each other. For example, in a cell where an existing CB was adjacent to a LacO locus without ABA treatment (Figure 4F, −200 s), ABA addition (between −200 s and 0 s, Figure 4F) led to rapid colocalization of the existing CB and the LacO locus, suggesting that the CRISPR-GO system can also mediate direct association between genomic loci and existing nuclear bodies, a phenomenon that has not yet been reported.

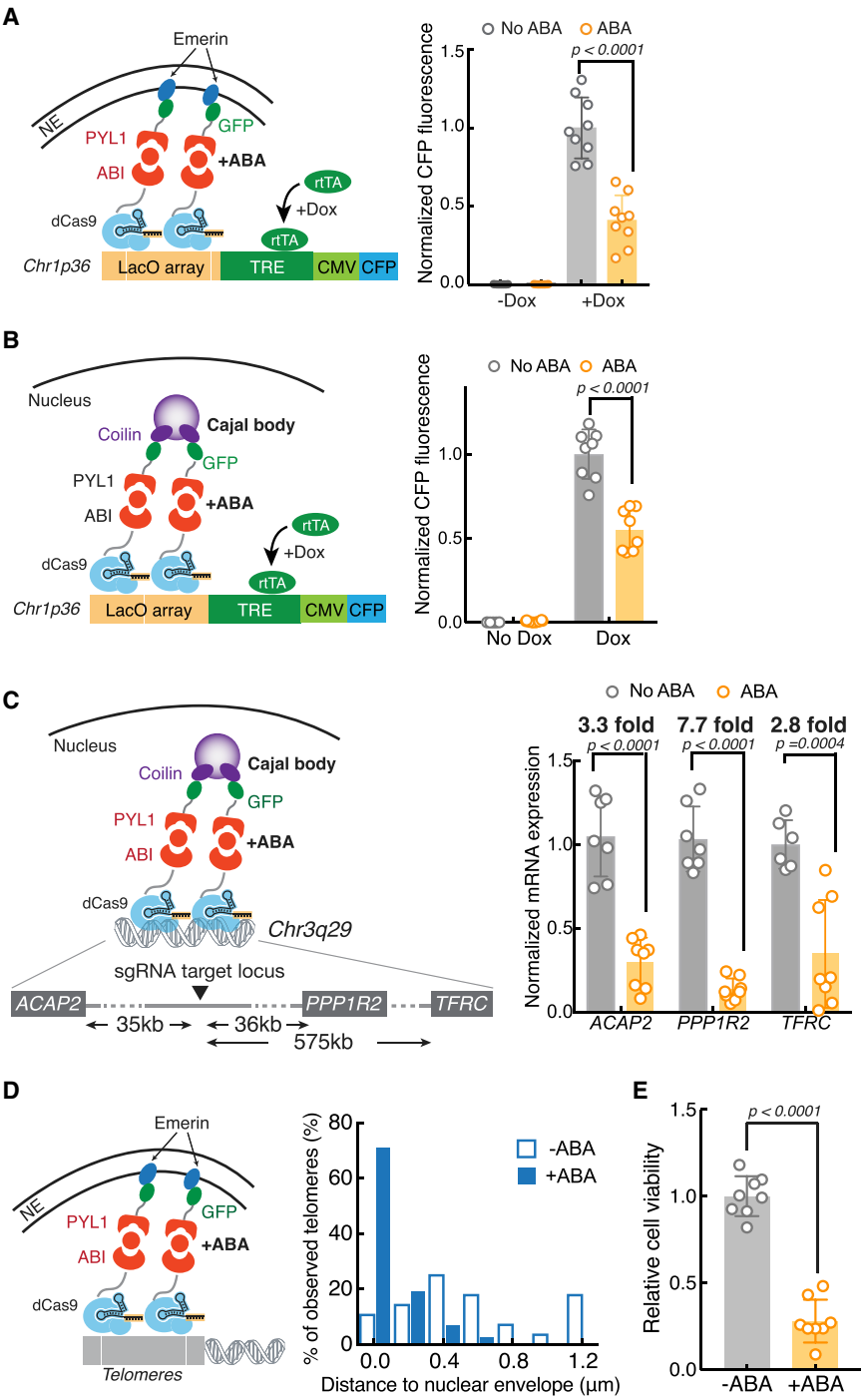

Figure 5. CRISPR-GO-Mediated Chromatin Repositioning Leads to Gene Expression Changes and Is Useful for the Study of Telomere Biology

(A and B) Repositioning targeted chromatin DNA to the nuclear periphery (A) or Cajal body (B) represses adjacent reporter gene expression. Left: schematics of the CRISPR-GO system to reposition a LacO repeat array, which is inserted adjacent to a Dox-inducible TRE promoter driving a CFP-SKL reporter gene. Right: comparisons of CFP reporter expression level using CRISPR-GO to reposition LacO loci to the nuclear periphery (A) or Cajal body (B) in ± Dox and ± ABA conditions. See Figure S4A and S4C for representative histograms and controls.

(C) Cajal body colocalization represses endogenous gene expression across long distances. Left: schematic of the CRISPR-GO system to colocalize the Chr3q29 locus to CBs. *ACAP2* is located 35 kb upstream of the sgRNA target site, *PPP1R2* is located 36 kb downstream, and *TFRC* is located 575 kb downstream. Right: gene expression measured by qRT-PCR using CRISPR-GO to colocalize Chr3 loci to CBs in ± ABA conditions. See Figure S4D for controls.

(D) Histograms of distances between telomeres and the nearest nuclear envelope point during interphase in example cells (Videos S1 and S2) in ± ABA conditions.

(E) Comparison of cell viability using the CRISPR-GO system to reposition telomeres to the nuclear envelope. For (A)–(C) and (E), data are represented as mean ± SD. See also Figures S4 and S5 and Videos S1 and S2.

CRISPR-GO-Mediated Relocalization of Genomic Loci to the Nuclear Periphery Led to Reduced Reporter Gene Expression

We examined whether CRISPR-GO-mediated repositioning of genomic loci to the nuclear periphery could influence gene expression. We first targeted the LacO locus in U2OS 2-6-3 cells, which is located upstream of a Doxycycline (Dox)-inducible TRE (Tetracycline responsive element)-CMV promoter that drives expression of a CFP reporter (Kumaran and Spector, 2008) (Figure 5A). We treated cells with ABA for 2 days, induced with Dox for 40 hr, and measured the CFP expression by flow cytometry. ABA-treated cells showed a consistent decrease in reporter gene expression compared to untreated cells (a reduction of 59%, Figures 5A and S4A). This gene-repression effect was similar to that from repositioning the LacO locus to the nuclear periphery by use of a LacI-Emerin fusion protein (Reddy et al., 2008). In the non-targeting sgRNA control group, no change was observed in reporter gene expression after ABA treatment (Figure S4A).

We next tested whether repositioning endogenous genomic loci to the nuclear periphery could alter gene expression. We repositioned the Chr3, *XIST*, and *CXCR4* loci to the nuclear periphery individually and performed qRT-PCR to detect changes in nearby gene expression (Chr3: *ACAP2* & *PPP1R2*; *CXCR4*; *XIST*). Surprisingly, we saw no evidence of gene expression change for these genes (e.g., *ACAP2* & *PPP1R2* in Figure S4B). Thus, it raises the question whether

repositioning-induced gene expression changes are locus-dependent.

Colocalization of Genomic Loci with CBs Repressed Expression of Reporter and Endogenous Genes

We investigated whether colocalization of LacO loci to CBs using the CRISPR-GO system in the U2OS 2-6-3 cell line was sufficient to influence adjacent gene expression (Figure 5B). We treated cells with ABA for 2 days, induced with Dox for 1 day and measured the CFP expression by flow cytometry. We observed a decrease in reporter gene expression in ABA-treated cells compared to untreated cells (an average reduction of 45%, Figures 5B and S4C). To confirm that this gene repression effect is target-specific, we tested a non-targeting sgRNA and observed a slight but insignificant decrease ($p>0.05$) of the reporter gene expression (Figure S4C).

We also studied whether colocalizing an endogenous genomic locus to CBs could alter distal gene expression. We induced colocalization of Chr3 with CBs (Figures 3E and 3F) and performed qRT-PCR to detect changes in distal gene expression after 4 days of ABA treatment. Interestingly, we observed significant repression of genes compared to untreated cells (Figure 5C). *ACAP2*, located about 35 kb upstream of the CB-targeting loci on Chr3, exhibited a 3.3 fold repression after ABA treatment, and *PPP1R2*, located about 36 kb downstream, exhibited a 7.7-fold repression. Moreover, another distal gene, *TFRC*, located about 575 kb downstream, also exhibited a 2.8-fold repression. As a control, we confirmed that there were no changes in expression of all three genes without a targeting sgRNA (Figure S4D). Together, these results show that targeted colocalization of a given genomic locus with CBs is able to repress long-distance gene expression. The long-distance effect stands in contrast to CRISPRi (CRISPR interference) or CRISPRa (CRISPR activation), which only cause perturbations in gene expression at very short distances (usually less than a few kilobases) from the dCas9 binding site (Gilbert et al., 2014). The ability of CRISPR-GO to mediate distal gene repression may provide a new means of synthetic gene regulation.

CRISPR-GO-Mediated Telomere Repositioning Altered Cellular Phenotypes

We used the CRISPR-GO system to investigate how telomere reorganization to nuclear compartments affected cellular phenotypes. Among all tested genomic loci, the dynamics of telomeres are the best studied and are shown to be associated with the nuclear periphery and CBs at specific stages of the cell cycle (Crabbe et al., 2012; Jády et al., 2006). For example, telomeres are dynamically tethered to the nuclear envelope in post-mitotic cells and then relocate to the interior of the nucleus at G1 phase (Crabbe et al., 2012). Given the importance of telomeres for genome integrity, their interactions with nuclear compartments may have functional implications.

We used the CRISPR-GO system to retain telomeres to the nuclear periphery during interphase (Videos S1 and S2, Figure 5D). By using an Alamar blue cell viability assay, which measures metabolic activity of cells (Schreer et al., 2005), we found that the maintenance of telomeres at the nuclear periphery by CRISPR-GO led to a significant decrease in cell viability after 6 days of ABA treatment (72% reduction, Figure 5E). Cell cycle analysis showed that telomeres tethered to the nuclear periphery increased the percentage of cells at G0/G1 and reduced the percentage of cells at S and G2/M phase, suggesting G0/G1 arrest (Figure S4E). We also examined the effect of colocalizing telomeres with CBs and found that the colocalization increased cell viability (average 50% increase, Figures S5A–S5C). As a control, ABA treatment alone had no effect on cell viability in U2OS cells (Figure S5D). Altogether, these observations suggest that the position of telomeres relative to nuclear compartments plays an important role in cellular function.

DISCUSSION

We have expanded the CRISPR-Cas toolbox by developing a CRISPR-mediated genome organization (CRISPR-GO) system. The CRISPR-GO system enables programmable control of targeted genomic DNA positioning within the nucleus (Figure 6). We show that CRISPR-GO can efficiently target endogenous genomic loci to various nuclear compartments (the nuclear periphery, Cajal bodies, and PML bodies). The CRISPR-GO system is inducible and reversible, which allows us to interrogate the interaction dynamics between targeted chromatin DNA and nuclear compartments. Colocalization of genomic loci with the nuclear periphery or Cajal bodies alters adjacent reporter gene expression. Notably, colocalization of endogenous loci with Cajal bodies significantly represses distal gene expression (30–600 kb) from the target site. The CRISPR-GO method will facilitate a deeper understanding of the functional role of spatio-temporal genome organization.

CRISPR-GO Provides a Programmable and Versatile Platform for Targeting Genomic Loci to Different Nuclear Compartments

The CRISPR-GO system can efficiently target specific genomic loci to the nuclear periphery, Cajal bodies, and PML bodies. The system can potentially be adapted to other nuclear compartments such as nucleoli, nuclear pore complexes, nuclear speckles, and heterochromatin (e.g., via heterochromatin protein 1α, Figure S5E) (Cheutin et al., 2003). Thus, CRISPR-GO is a versatile modular platform with great potential for future expansion to study other nuclear compartments.

CRISPR-GO allows programmable re-localization of genomic loci in a precise and targeted manner. The CRISPR-GO system efficiently targeted repetitive and non-repetitive chromatin loci on different chromosomes to nuclear compartments. Unlike the LacI-LacO system, the genomic target of the CRISPR-GO system can be flexibly defined by the base-pairing interactions between sgRNAs and the target DNA sequence, and simply altering a ~20nt region on the sgRNA allows us to target a different genomic locus. This programmable feature allows one to use CRISPR-GO to potentially target a variety of genomic elements, including protein-coding genes, non-coding RNA genes, and regulatory elements. In contrast, the LacO-LacI technique is not suitable for programmable genomic

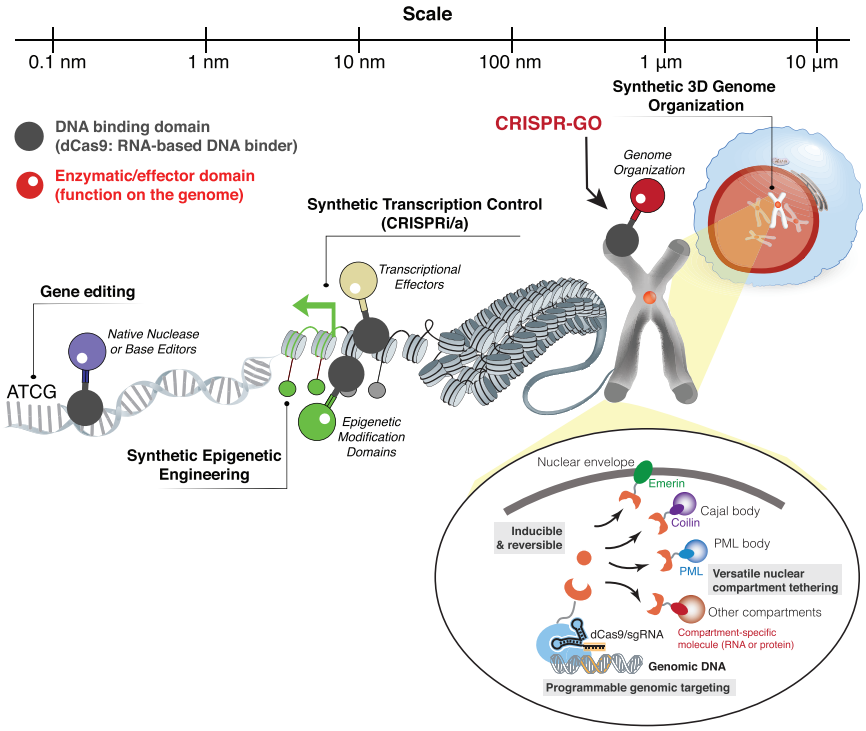

CRISPR-GO system for genome organization

Figure 6. The CRISPR-GO System Enables Programmable Control of 3D Genome Organization and Expands CRISPR-Cas Applications for Genome Engineering

The CRISPR-GO method allows for programmable control of 3D genome organization over micrometers, which expands the utility of the CRISPR-Cas toolbox beyond gene editing, transcriptional regulation, and epigenetic modifications. See also Figure S6.

targeting, since it can only be used with well-characterized cell lines that contain a highly repetitive LacO array. The versatility of the CRISPR-GO system offers a major technological advantage over the LacO-LacI method for studying nuclear organization.

The overall ease of targeting a new locus with CRISPR-GO will facilitate broader studies of the relationship between perturbations in 3D genome organization and changes in cellular phenotypes. Repetitive genomic loci can be targeted using a single sgRNA that has multiple targets within a defined genomic region. Given that the repetitive sequences are abundant in the human genome (Figure S6) (de Koning et al., 2011), they provide candidates for large-scale screening experiments to systematically study the relationship between genome organization and cellular phenotype. In addition, non-repetitive genomic loci can be targeted by using multiple sgRNAs or a single sgRNA. The efficiency of CRISPR-GO may be affected by sgRNA designs and chromatin accessibility, so choosing a sgRNA that has been validated for other CRISPR-Cas applications (e.g., CRISPRi/a) will likely maximize the chance of success.

CRISPR-GO Is Inducible and Reversible, Allowing for the Study of Dynamic Genomic Repositioning Processes throughout the Cell Cycle

CRISPR-GO is inducible and reversible, allowing us to study the real-time dynamics of genomic repositioning while potentially preventing any adverse effects from continuously repositioning chromatin DNA to a given nuclear compartment. We showed that relocalization of endogenous genomic loci to the nuclear periphery occurred in both a mitosis-dependent and -independent manner. During mitosis, the nuclear membrane breaks down in prometaphase (Smoyer and Jaspersen, 2014), which may facilitate interactions between genomic loci and the nuclear membrane. Nuclear periphery tethering during interphase may rely on the proximity of targeted loci to the nuclear periphery, and genomic loci that are distal to the nuclear periphery may be less likely to be tethered through a mitosis-independent manner. The mechanism of CRISPR-GO-mediated genomic repositioning during different phases of the cell cycle warrants future study, and this may provide insights into the underpinnings of genome organization throughout the cell cycle.

CRISPR-GO Can Target Genomic Loci to Existing CBs and Can Also Mediate Rapid Formation of *De Novo* CBs, Providing a Tool to Study Nuclear Body Dynamics

Colocalization between genomic loci and CBs occurred at a much faster rate (within minutes), when compared to the relatively slower repositioning to the nuclear periphery (within hours). This is likely because CB components are more diffuse throughout the nucleus. We observed that colocalization between CBs and the target genomic loci occurred in two ways: (1) through rapid formation of *de novo* CBs at the genomic loci, and (2) through relocalization of existing CBs to targeted genomic loci, a phenomenon which has not been reported. Previous work suggests that CBs are formed by phase separation (Zhu and Brangwynne, 2015). It is possible that recruiting nuclear body components (e.g., Coilin for CBs) to targeted genomic loci may generate synthetic phase separation, which merits future investigation.

CRISPR-GO-Mediated Genomic Re-organization Affects Gene Expression

Previous work reported different effects on gene expression after tethering LacO loci to the nuclear periphery. Kumaran and Spector observed no change in transcription after recruiting LacO repeats to the nuclear periphery by LacI-Lamin B (Kumaran and Spector, 2008). In contrast, Reddy et al. (2008) showed that tethering LacO repeats to the nuclear periphery by LacI-Emerin

caused repression of adjacent genes. As in Reddy et al., our CRISPR-GO system showed that repositioning the reporter gene to Emerin caused gene repression. The observed difference in gene expression changes may be explained by the use of different recruiting molecules or other experimental conditions, which may reposition genes to different periphery locations with distinct repressive or activating complexes. We also performed qRT-PCR after recruiting endogenous genomic loci to the nuclear periphery, but none of the adjacent genes we tested showed changes in mRNA expression. Thus, it raises the question whether gene expression changes induced by repositioning are locus-dependent. Future studies could investigate the effects of genomic repositioning on gene expression on the single-cell level and potential compensatory effects of non-repositioned alleles. CRISPR-GO could provide a systematic approach to test diverse genomic loci for mapping the correlation between nuclear positioning and gene expression.

Repression of both reporter and endogenous genes was detected after CRISPR-GO-mediated colocalization of chromatin loci to CBs. Importantly, targeted colocalization of CBs with endogenous loci repressed gene expression across long distances (30–600 kb). To our knowledge, the observed gene repression after targeting a genomic locus to CBs has not yet been reported. The CRISPRi/a methods function by recruiting transcriptional effectors that mostly affect expression of local genes within a few kilobases around the target site (Gilbert et al., 2014). Thus, CRISPR-GO provides a novel method for regulating gene expression over long distances. It is possible that recruiting a CB to a given chromatin locus by CRISPR-GO encompasses a large chromatin region and disfavors transcription, which causes distal gene repression. Another possibility is that the genes we targeted were close in 3D space, though no evident looping between these genes and our sgRNA targeting region has been detected by 3C-based techniques (e.g., ChIA-PET and HiChiP) in multiple studied cells (3D Genome Database: http://promoter.bx.psu.edu/hi-c). CB colocalization may also alter local chromatin conformation through disrupting looping and promoter-enhancers interactions, and thus affect gene transcription over long distances. Further investigation is required to study how CRISPR-GO affects the transcription, epigenetic status, and local chromatin structure of nearby and distal genes. Altogether, the ability to use CRISPR-GO to control repositioning of target DNA to diverse nuclear compartments offers a systematic approach to investigate these questions and provides a novel method for programmable gene regulation.

STAR★METHODS

Detailed methods are provided in the online version of this paper and include the following:

- KEY RESOURCES TABLE
- CONTACT FOR REAGENT AND RESOURCE SHARING
- EXPERIMENTAL MODEL AND SUBJECT DETAILS
  - Cell culture
- METHOD DETAILS
  - Plasmids construction
  - Genomic loci targeted by CRISPR-GO system
  - Generation of stable cell lines
  - Lentivirus production
  - Live-cell genomic imaging
  - FISH
  - Immunostaining of nuclear body markers
  - Chemical induction and reversal experiment
  - Cell cycle synchronization
  - Microscopy and real-time imaging
  - Image processing and analysis
  - Flow cytometry fluorescence assays
  - qRT-PCR
  - Cell viability assay
  - Cell cycle cytometry analysis
  - Identification of repetitive sequences
- QUANTIFICATION AND STATISTICAL ANALYSIS
  - Quantification of genomic repositioning
  - Short-term genomic tracking
  - Statistical Analysis

SUPPLEMENTAL INFORMATION

Supplemental Information includes six figures, two tables, and two videos and can be found with this article online at https://doi.org/10.1016/j.cell.2018.09.013.

ACKNOWLEDGMENTS

The authors thank the Cell Sciences Imaging Facility at Stanford University and Cedric Espenel for microscope usage and assistance. We acknowledge David L. Spector in Cold Spring Harbor Laboratory for providing U2OS 2-6-3 cells, Luke Lavis at the Janelia Research Campus for providing the JF549-HaloTag ligand, and David M. Chenoweth at the University of Pennsylvania for providing the TMP-HTag ligand. We thank Yodai Takei in Long Cai's lab at California Institute of Technology for help on the FISH probe design. We thank Paul J. Vorster and Timothy R. Abbott for proofreading the manuscript. L.S.Q. acknowledges support from Pew Scholar Program and Alfred P. Sloan Foundation. This work was supported by NIH Director's Early Independence Award (grant OD017887, L.S.Q.), NIH 4D Nucleome Imaging Tool U01 (grant EB021240, L.S.Q.), and a gift fund from Li Ka Shing Foundation.

AUTHOR CONTRIBUTIONS

H.W. and L.S.Q. conceived of the idea. H.W. and L.S.Q. planned the experiments. H.W., X.X., C.M.N., Y.L., Y.G., and N.H.K. performed the experiments. H.W., C.M.N., X.L., T.D., and L.S.Q. analyzed the data. H.W., M.L.R., and L.S.Q. wrote the manuscript. All authors read and commented on the manuscript.

DECLARATION OF INTERESTS

The authors have filed a related patent (US Provisional Patent # 62/722,684).

Received: May 16, 2018
Revised: August 9, 2018
Accepted: September 10, 2018
Published: October 11, 2018

REFERENCES

Ballister, E.R., Aonbangkhen, C., Mayo, A.M., Lampson, M.A., and Chenoweth, D.M. (2014). Localized light-induced protein dimerization in living cells using a photocaged dimerizer. Nat. Commun. *5*, 5475.

Barrangou, R., Fremaux, C., Deveau, H., Richards, M., Boyaval, P., Moineau, S., Romero, D.A., and Horvath, P. (2007). CRISPR provides acquired resistance against viruses in prokaryotes. Science *315*, 1709–1712.

Benson, G. (1999). Tandem repeats finder: a program to analyze DNA sequences. Nucleic Acids Res. *27*, 573–580.

Berk, J.M., Tifft, K.E., and Wilson, K.L. (2013). The nuclear envelope LEM-domain protein emerin. Nucleus *4*, 298–314.

Bickmore, W.A. (2013). The spatial organization of the human genome. Annu. Rev. Genomics Hum. Genet. *14*, 67–84.

Chen, B., Gilbert, L.A., Cimini, B.A., Schnitzbauer, J., Zhang, W., Li, G.W., Park, J., Blackburn, E.H., Weissman, J.S., Qi, L.S., and Huang, B. (2013). Dynamic imaging of genomic loci in living human cells by an optimized CRISPR/Cas system. Cell *155*, 1479–1491.

Cheutin, T., McNairn, A.J., Jenuwein, T., Gilbert, D.M., Singh, P.B., and Misteli, T. (2003). Maintenance of stable heterochromatin domains by dynamic HP1 binding. Science *299*, 721–725.

Clowney, E.J., LeGros, M.A., Mosley, C.P., Clowney, F.G., Markenskoff-Papadimitriou, E.C., Myllys, M., Barnea, G., Larabell, C.A., and Lomvardas, S. (2012). Nuclear aggregation of olfactory receptor genes governs their monogenic expression. Cell *151*, 724–737.

Cong, L., Ran, F.A., Cox, D., Lin, S., Barretto, R., Habib, N., Hsu, P.D., Wu, X., Jiang, W., Marraffini, L.A., and Zhang, F. (2013). Multiplex genome engineering using CRISPR/Cas systems. Science *339*, 819–823.

Crabbe, L., Cesare, A.J., Kasuboski, J.M., Fitzpatrick, J.A., and Karlseder, J. (2012). Human telomeres are tethered to the nuclear envelope during postmitotic nuclear assembly. Cell Rep. *2*, 1521–1529.

de Koning, A.P., Gu, W., Castoe, T.A., Batzer, M.A., and Pollock, D.D. (2011). Repetitive elements may comprise over two-thirds of the human genome. PLoS Genet. *7*, e1002384.

Dekker, J., Rippe, K., Dekker, M., and Kleckner, N. (2002). Capturing chromosome conformation. Science *295*, 1306–1311.

Finlan, L.E., Sproul, D., Thomson, I., Boyle, S., Kerr, E., Perry, P., Ylstra, B., Chubb, J.R., and Bickmore, W.A. (2008). Recruitment to the nuclear periphery can alter expression of genes in human cells. PLoS Genet. *4*, e1000039.

Gall, J.G. (2000). Cajal bodies: the first 100 years. Annu. Rev. Cell Dev. Biol. *16*, 273–300.

Gao, Y., Xiong, X., Wong, S., Charles, E.J., Lim, W.A., and Qi, L.S. (2016). Complex transcriptional modulation with orthogonal and inducible dCas9 regulators. Nat. Methods *13*, 1043–1049.

Gilbert, L.A., Larson, M.H., Morsut, L., Liu, Z., Brar, G.A., Torres, S.E., Stern-Ginossar, N., Brandman, O., Whitehead, E.H., Doudna, J.A., et al. (2013). CRISPR-mediated modular RNA-guided regulation of transcription in eukaryotes. Cell *154*, 442–451.

Gilbert, L.A., Horlbeck, M.A., Adamson, B., Villalta, J.E., Chen, Y., Whitehead, E.H., Guimaraes, C., Panning, B., Ploegh, H.L., Bassik, M.C., et al. (2014). Genome-Scale CRISPR-Mediated Control of Gene Repression and Activation. Cell *159*, 647–661.

Grimm, J.B., English, B.P., Chen, J., Slaughter, J.P., Zhang, Z., Revyakin, A., Patel, R., Macklin, J.J., Normanno, D., Singer, R.H., et al. (2015). A general method to improve fluorophores for live-cell and single-molecule microscopy. Nat Methods *12*, 244–250, 243 p following 250.

Guan, J., Liu, H., Shi, X., Feng, S., and Huang, B. (2017). Tracking Multiple Genomic Elements Using Correlative CRISPR Imaging and Sequential DNA FISH. Biophys. J. *112*, 1077–1084.

Hilton, I.B., D'Ippolito, A.M., Vockley, C.M., Thakore, P.I., Crawford, G.E., Reddy, T.E., and Gersbach, C.A. (2015). Epigenome editing by a CRISPR-Cas9-based acetyltransferase activates genes from promoters and enhancers. Nat. Biotechnol. *33*, 510–517.

Jády, B.E., Richard, P., Bertrand, E., and Kiss, T. (2006). Cell cycle-dependent recruitment of telomerase RNA and Cajal bodies to human telomeres. Mol. Biol. Cell *17*, 944–954.

Jinek, M., Chylinski, K., Fonfara, I., Hauer, M., Doudna, J.A., and Charpentier, E. (2012). A programmable dual-RNA-guided DNA endonuclease in adaptive bacterial immunity. Science *337*, 816–821.

Kaiser, T.E., Intine, R.V., and Dundr, M. (2008). De novo formation of a subnuclear body. Science *322*, 1713–1717.

Kosak, S.T., Skok, J.A., Medina, K.L., Riblet, R., Le Beau, M.M., Fisher, A.G., and Singh, H. (2002). Subnuclear compartmentalization of immunoglobulin loci during lymphocyte development. Science *296*, 158–162.

Kumaran, R.I., and Spector, D.L. (2008). A genetic locus targeted to the nuclear periphery in living cells maintains its transcriptional competence. J. Cell Biol. *180*, 51–65.

Langer-Safer, P.R., Levine, M., and Ward, D.C. (1982). Immunological method for mapping genes on Drosophila polytene chromosomes. Proc. Natl. Acad. Sci. USA *79*, 4381–4385.

Liang, F.S., Ho, W.Q., and Crabtree, G.R. (2011). Engineering the ABA plant stress pathway for regulation of induced proximity. Sci. Signal. *4*, rs2.

Ma, H., Tu, L.C., Naseri, A., Huisman, M., Zhang, S., Grunwald, D., and Pederson, T. (2016). Multiplexed labeling of genomic loci with dCas9 and engineered sgRNAs using CRISPRainbow. Nat. Biotechnol. *34*, 528–530.

Mali, P., Yang, L., Esvelt, K.M., Aach, J., Guell, M., DiCarlo, J.E., Norville, J.E., and Church, G.M. (2013). RNA-guided human genome engineering via Cas9. Science *339*, 823–826.

Mao, Y.S., Zhang, B., and Spector, D.L. (2011). Biogenesis and function of nuclear bodies. Trends Genet. *27*, 295–306.

Morgan, S.L., Mariano, N.C., Bermudez, A., Arruda, N.L., Wu, F., Luo, Y., Shankar, G., Jia, L., Chen, H., Hu, J.F., et al. (2017). Manipulation of nuclear architecture through CRISPR-mediated chromosomal looping. Nat. Commun. *8*, 15993.

Qi, L.S., Larson, M.H., Gilbert, L.A., Doudna, J.A., Weissman, J.S., Arkin, A.P., and Lim, W.A. (2013). Repurposing CRISPR as an RNA-guided platform for sequence-specific control of gene expression. Cell *152*, 1173–1183.

Reddy, K.L., Zullo, J.M., Bertolino, E., and Singh, H. (2008). Transcriptional repression mediated by repositioning of genes to the nuclear lamina. Nature *452*, 243–247.

Reineke, E.L., and Kao, H.Y. (2009). Targeting promyelocytic leukemia protein: a means to regulating PML nuclear bodies. Int. J. Biol. Sci. *5*, 366–376.

Schindelin, J., Arganda-Carreras, I., Frise, E., Kaynig, V., Longair, M., Pietzsch, T., Preibisch, S., Rueden, C., Saalfeld, S., Schmid, B., et al. (2012). Fiji: an open-source platform for biological-image analysis. Nat. Methods *9*, 676–682.

Schreer, A., Tinson, C., Sherry, J.P., and Schirmer, K. (2005). Application of Alamar blue/5-carboxyfluorescein diacetate acetoxymethyl ester as a noninvasive cell viability assay in primary hepatocytes from rainbow trout. Anal. Biochem. *344*, 76–85.

Shpargel, K.B., Ospina, J.K., Tucker, K.E., Matera, A.G., and Hebert, M.D. (2003). Control of Cajal body number is mediated by the coilin C-terminus. J. Cell Sci. *116*, 303–312.

Smogorzewska, A., and de Lange, T. (2002). Different telomere damage signaling pathways in human and mouse cells. EMBO J. *21*, 4338–4348.

Smoyer, C.J., and Jaspersen, S.L. (2014). Breaking down the wall: the nuclear envelope during mitosis. Curr. Opin. Cell Biol. *26*, 1–9.

Takei, Y., Shah, S., Harvey, S., Qi, L.S., and Cai, L. (2017). Multiplexed Dynamic Imaging of Genomic Loci by Combined CRISPR Imaging and DNA Sequential FISH. Biophys. J. *112*, 1773–1776.

Tanenbaum, M.E., Gilbert, L.A., Qi, L.S., Weissman, J.S., and Vale, R.D. (2014). A protein-tagging system for signal amplification in gene expression and fluorescence imaging. Cell *159*, 635–646.

Tinevez, J.Y., Perry, N., Schindelin, J., Hoopes, G.M., Reynolds, G.D., Laplantine, E., Bednarek, S.Y., Shorte, S.L., and Eliceiri, K.W. (2017). TrackMate: An open and extensible platform for single-particle tracking. Methods *115*, 80–90.

van Steensel, B., and Belmont, A.S. (2017). Lamina-Associated Domains: Links with Chromosome Architecture, Heterochromatin, and Gene Repression. Cell *169*, 780–791.

Vernier, M., Bourdeau, V., Gaumont-Leclerc, M.F., Moiseeva, O., Bégin, V., Saad, F., Mes-Masson, A.M., and Ferbeyre, G. (2011). Regulation of E2Fs and senescence by PML nuclear bodies. Genes Dev. *25*, 41–50.

Williams, R.R., Azuara, V., Perry, P., Sauer, S., Dvorkina, M., Jørgensen, H., Roix, J., McQueen, P., Misteli, T., Merkenschlager, M., and Fisher, A.G. (2006). Neural induction promotes large-scale chromatin reorganisation of the Mash1 locus. J. Cell Sci. *119*, 132–140.

Yu, M., and Ren, B. (2017). The Three-Dimensional Organization of Mammalian Genomes. Annu. Rev. Cell Dev. Biol. *33*, 265–289.

Zhu, L., and Brangwynne, C.P. (2015). Nuclear bodies: the emerging biophysics of nucleoplasmic phases. Curr. Opin. Cell Biol. *34*, 23–30.

Zuleger, N., Kelly, D.A., Richardson, A.C., Kerr, A.R., Goldberg, M.W., Goryachev, A.B., and Schirmer, E.C. (2011). System analysis shows distinct mechanisms and common principles of nuclear envelope protein dynamics. J. Cell Biol. *193*, 109–123.

STAR★METHODS

KEY RESOURCES TABLE

REAGENT or RESOURCE	SOURCE	IDENTIFIER
Antibodies		
Mouse monoclonal Anti-SMN/Gemin 1 [2B1]	Santa Cruz	Cat.# sc-32313; RRID: AB_627931
Rabbit polyclonal Anti-SP100 antibody	Abcam	Cat.# ab43151; RRID:AB_1143037
Mouse monoclonal Anti-Fibrillarin [38F3]	Abcam	Cat.# ab4566; RRID:AB_304523
Mouse monoclonal Gemin2 Antibody (3F8)	Santa Cruz	Cat.# sc-32806; RRID:AB_627669
Donkey anti-Rabbit IgG (H+L), Alexa Fluor 647	ThermoFisher	Cat.# A-31573; RRID:AB_2536183
Donkey anti-Mouse IgG (H+L), Alexa Fluor 594	ThermoFisher	Cat.# A-21203; RRID:AB_141633
Chemicals, Peptides, and Recombinant Proteins		
Abscisic acid	Sigma-Aldrich	Cat.# A1049
JF549-HaloTag	Grimm et al., 2015	N/A
Alamarblue cell viability reagent	Thermo Fisher	Cat.# DAL1025
Hoechst 33342, Trihydrochloride, Trihydrate	Thermo Fisher	H3570
Experimental Models: Cell Lines		
Human: U-2 OS cell line	ATCC	Cat.# HTB-96; RRID:CVCL_0042
Human: Hela cell line	Sigma	Cat. # 93021013; RRID:CVCL_0030
U2OS 2-6-3 cell	Kumaran and Spector, 2008	N/A
HEK293T	ATCC	Cat.# CRL-3216; RRID:CVCL_0063
Oligonucleotides		
PrimePCR™ SYBR® Green Assay: PPP1R2, Human	BioRad	Cat.# 10025636
PrimePCR™ SYBR® Green Assay: ACAP2, Human	BioRad	Cat.# 10025636
PrimePCR™ SYBR® Green Assay: TFRC, Human	BioRad	Cat.# 10025636
SgRNAs targeting Repetitive regions: See Table S1	This paper	N/A
SgRNAs targeting Non-Repetitive genes: See Table S2	This paper	N/A
LacO targeting Alexa Fluor 647 FISH probe 5'-TTGTTATCCGCTC ACAATTCCACATGTGGCCACAAA-3'	This paper	N/A
Chr7 loci targeting FISH probe 5'-Cy3-CCCACACTCTC ACCATAAGAGC-3'	Guan et al., 2017	N/A
ChrX loci targeting FISH probe 5-Cy3-TTGCCTTGTG CCTTGCCTTGC-3'	Guan et al., 2017	N/A
CXCR4 gene FISH probe	Empire Genomics	Cat.# CXCR4-20-RE
PTEN gene FISH probe	Cell Line Genetics	PTEN gene FISH probe, red
XIST gene FISH probe	Cell Line Genetics	XIST gene FISH probe, red
Recombinant DNA		
pHR-SFFV-ABI-tagBFP-dCas9	Gao et al., 2016	N/A
Emerin pEGFP-C1 (637)	Zuleger et al., 2011	Addgene plasmid #61993
pEGFP-Coilin	Shpargel et al., 2003	Addgene plasmid #36906
pLPC-Flag-PML-IV	Vernier et al., 2011	Addgene plasmid #62804
GFP-HP1α	Cheutin et al., 2003	Addgene plasmid #17652
SV-ABAactDA	Liang et al., 2011	Addgene plasmid #38247
pERB221	Ballister et al., 2014	Addgene plasmid #61502
pLPC-NFLAG TRF1	Smogorzewska and de Lange, 2002	Addgene plasmid #16058
pSLQ1651-sgTelomere(F+E)	Chen et al., 2013	Addgene plasmid #51024
pHR-PGK-ABI-dCas9-P2A-mCherry	This paper	N/A
pHR-PGK-ABI-dCas9-P2A-Puro	This paper	N/A

(*Continued on next page*)

Continued

REAGENT or RESOURCE	SOURCE	IDENTIFIER
pHR-PGK-ABI-tagBFP-dCas9	This paper	N/A
pHR-TRE3G-dCas9-HaloTag	This paper	N/A
pHR-SFFV-PYL1-sfGFP-Emerin	This paper	N/A
pHR-PGK-PYL1-sfGFP-Coilin	This paper	N/A
pHR-TRE3G-PYL1-sfGFP-PML	This paper	N/A
pHR-TRE3G-dCas9-EGFP-HaloTag	This paper	N/A
pHR-SFFV-DHFR-mCherry-Emerin	This paper	N/A
pHR-U6-sgRNA-CMV-puro	This paper	N/A
pHR-U6-sgTel-CMV-puro-P2A-TRF1-mCherry	This paper	N/A
Software and Algorithms		
Fiji (image J)	Schindelin et al., 2012	https://fiji.sc
TrackMate plugin	Tinevez et al., 2017	https://imagej.net/TrackMate
Tandem Repeats Finder	Benson, 1999	N/A
Prism 7	GraphPad	https://www.graphpad.com
Imaris 9.1.2	Bitplane	http://www.bitplane.com
MetaMorph	Molecular devices, CA	RRID:SCR_002368
Rstudio	Rstudio	https://www.rstudio.com/
FlowJo	FlowJo.LLC	https://www.flowjo.com

CONTACT FOR REAGENT AND RESOURCE SHARING

Further information and requests for resources and reagents should be directed to and will be fulfilled by the Lead Contact, Lei S. Qi (stanley.qi@stanford.edu).

EXPERIMENTAL MODEL AND SUBJECT DETAILS

Cell culture

The U2OS (human bone osteosarcoma epithelial, female) cells, and HEK293T cells (human embryonic kidney epithelial, female) and HeLa cells (Human cervix epitheloid carcinoma, female) were cultured in DMEM with GlutaMAX (Life Technologies) in 10% Tet-system-approved FBS (Life Technologies). U2OS 2-6-3 cell line was a gift from Dr. David L. Spector (Cold Spring Harbor Laboratory) and were cultured in the same condition (Kumaran and Spector, 2008). All cells were cultured at 37°C and 5% CO_2 in a humidified incubator.

METHOD DETAILS

Plasmids construction

pHR-SFFV-PYL1-sfGFP-Emerin was cloned by replacing scFv sequence in pHR-SFFV-scFv-sfGFP plasmid (Tanenbaum et al., 2014) with PYL1 and inserting Emerin after sfGFP. Emerin (encoded by the *EMD* gene) was cloned from Emerin pEGFP-C1 (637) (Addgene plasmid 61993), a gift from Eric Schirmer (Zuleger et al., 2011). pHR-SFFV-PYL1-sfGFP-Coilin was cloned from the pHR-SFFV-PYL1-sfGFP-Emerin plasmid, by replacing Emerin with Coilin. Coilin was cloned from pEGFP-Coilin (Addgene plasmid 36906), a gift from Dr. Greg Matera (Shpargel et al., 2003). pHR-PGK-PYL1-sfGFP-Coilin was cloned by replacing the SFFV promoter in pHR-SFFV-PYL1-sfGFP-Coilin plasmid with the PGK promoter. pHR-TRE3G-PYL1-sfGFP-PML and pHR-TRE3G-PYL1-sfGFP-HP1α was cloned by replacing the PGK promoter with the TRE3G promoter and replacing Coilin with PML and HP1α in the pHR-PGK-PYL1-sfGFP-Coilin plasmid. PML was cloned from pLPC-Flag-PML-IV (addgene plasmid 62804), a gift from Gerardo Ferbeyre (Vernier et al., 2011). HP1α was cloned from GFP-HP1α (Addgene plasmid 17652), a gift from Tom Misteli (Cheutin et al., 2003).

pHR-SFFV-ABI-tagBFP-dCas9 was described before (Gao et al., 2016). pHR-PGK-ABI-tagBFP-dCas9 was cloned by replacing the SFFV promotor with the PGK promoter in pHR-SFFV-ABI-tagBFP-dCas9. pHR-PGK-ABI-dCas9-P2A-Cherry, or pHR-PGK-ABI-dCas9-P2A-Puro was cloned by replacing SFFV with PGK promoter, deleting tagBFP and adding P2A-mCherry or P2A-Puro in pHR-SFFV-ABI-tagBFP-dCas9. ABI and PYL1 were cloned from Addgene plasmid 38247 (Liang et al., 2011), a gift from Dr. Gerald Crabtree, Stanford.

pHR-TRE3G-dCas9-HaloTag was cloned by replacing $SunTag_{10}$-P2A-mCherry with HaloTag in the plasmid pHR-TRE3G-dCas9-HA-$SunTag_{10}$-P2A-mCherry (Tanenbaum et al., 2014). pHR-TRE3G-dCas9-EGFP-HaloTag was cloned by inserting HaloTag after EGFP in pHR-TRE3G-dCas9-EGFP (Chen et al., 2013). pHR-SFFV-DHFR-mCherry-Emerin was cloned by replacing PYL1-sfGFP sequence in pHR-SFFV-PYL1-sfGFP-Emerin with mCherry-DHFR. HaloTag and mCherry-DHFR was cloned from pERB221 (Addgene plasmid 61502), a gift from David Chenoweth and Michael Lampson (Ballister et al., 2014).

All sgRNAs were cloned into the pHR-U6-sgTel-CMV-puro-P2A-mCherry vector after removing P2A-mCherry (pSLQ1651-sgTelomere(F+E), Chen et al., 2013, addgene plasmid 51024). TRF1-mCherry was cloned into the pHR-U6-sgTel-CMV-puro-P2A-mCherry vector in place of mCherry. TRF1 was cloned from pLPC-NFLAG TRF1, a gift from Dr. Titia de Lange (Smogorzewska and de Lange, 2002) (Addgene plasmid 16058).

Genomic loci targeted by CRISPR-GO system

We tested the efficacy of the CRISPR-GO system by targeting different chromosomal regions in human cells. Both repetitive regions and non-repetitive genes were tested (Figure S2). The endogenous repetitive regions include Chr3q29: 195478324-195506987; Chr13q34: 112277485-112319169; Chr7q36.3: 158329969-158342636; ChrXp21.2: 30788554-30806701 and telomeres (Guan et al., 2017; Ma et al., 2016). A synthetic LacO repeat inserted at Chr1p36 in U2OS 2-6-3 cells was also used for targeting (Kumaran and Spector, 2008). For repetitive regions, a single sgRNA design was used to target multiple repeats within the selected region (Table S1) (Chen et al., 2013; Guan et al., 2017; Ma et al., 2016). Non-repetitive genes include *CXCR4* located at Chr2q22.1, *XIST* located at ChrXq13.2, and *PTEN* located at Chr10q23.31. Multiple sgRNAs were designed to target non-repetitive genes at gene bodies and upstream regions (Table S2).

Generation of stable cell lines

To create stable CRISPR-GO cell lines that targets endogenous loci to nuclear compartments, U2OS cells were plated into 24-well plates, cultured for 24 hr to reach 50% confluency, and then transduced with lentivirus. Cells transduced by lentivirus expressing PYL1-sfGFP-Emerin, PYL1-sfGFP-Coilin, PYL1-sfGFP-PML, or PYL1-sfGFP-HP1α and ABI-tagBFP-dCas9 were sorted by fluorescence activated cell sorting (FACS) at Stanford shared FACS facility for cells that are BFP and GFP positive to create stable cell lines. For nuclear periphery targeting experiments, cells of high BFP and GFP expression level were selected. For other nuclear compartment targeting, cells of low BFP and GFP expression level were selected. CRISPR-GO cell lines were then transduced with lentivirus expressing targeting sgRNAs, and sgRNA-positive cells were selected with puromycin at 2μg/ml.

In order to target LacO loci in U2OS 2-6-3 cell lines (Kumaran and Spector, 2008), cells were transduced by a lentivirus mixture containing PYL1-sfGFP-Emerin or PYL1-sfGFP-Coilin and ABI-dCas9-P2A-mCherry. Cells were subsequently sorted for GFP and mCherry positive cells to create stable cell lines. SgRNA positive cells were selected with puromycin at 2μg/ml. To quantify the efficacy of LacO nuclear periphery repositioning by CRISPR imaging, U2OS 2-6-3 cells were transduced with lentivirus coding ABI-dCas9-P2A-Puro instead of ABI-dCas9-P2A-mCherry, and treated with puromycin at 2μg/ml for positive selection.

Lentivirus production

To produce lentivirus, HEK293T cells were transiently transfected with pHR constructs, and packaging plasmids pCMV-dR8.91 and PMD2.G. Lentivirus was collected 72 hr after transfection by filtering supernatant through 0.45μm filters. When necessary, virus supernatant was concentrated using Lenti-X concentrator at 4°C overnight, and centrifuged at 1500 g for 30min at 4°C to collect virus pellets. The pellets were re-suspended in cold culture medium, and directly added to cells or frozen at −80°C.

Live-cell genomic imaging

CRISPR imaging was performed to visualize the localization of Chr3, Chr13 and LacO loci in living cells (Figure S1C). For live-cell CRISPR imaging, stable cell lines expressing CRISPR-GO components were transduced by lentivirus encoding the dCas9-HaloTag and targeting sgRNAs in Ibidi 24-well μ-plate (Ibidi, Inc). Targeted genomic loci were labeled by dCas9-HaloTag and stained by JF549-HaloTag ligand at 0.1-0.5μM for 15min at 37°C in culture media. After staining, cells were washed with culture medium twice, and then incubated in phenol-red free culture medium during microscopy. JF549-HaloTag was a gift from Dr. Luke Lavis in Janelia Research Campus (Grimm et al., 2015). Telomere loci were labeled in live cells by expression of TRF1-mCherry, a telomere binding protein.

FISH

Other genomic loci were labeled by 3D DNA FISH in fixed cells. LacO, Chr7 and ChrX loci were labeled using synthesized fluorescent nucleotide probes (Integrated DNA Technologies, Redwood City, CA). LacO loci were labeled with an Alexa Fluor 647 labeled FISH probe (5′-TTGTTATCCGCTCACAATTCCACATGTGGCCACAAA-3′) at 10nM concentration. Chr7 loci were labeled by a Cy3 labeled FISH probe (5′-Cy3-CCCACACTCTCACCATAAGAGC-3′) at 200nM, and ChrX loci were labeled by (5-Cy3-TTGCCTTGTGCCTTGCCTTGC-3′) at 200nM (Guan et al., 2017). Commercial FISH probes were used according to the manufacturers protocols to target *CXCR4, PTEN* and *XIST.* The *CXCR4* FISH probe was purchased from Empire Genomics (Cat.# CXCR4-20-RE).The *PTEN* and *XIST* FISH probes were purchased from Cell Line Genetics (*PTEN* gene FISH probe, red and *XIST* gene FISH probe, red).

Oligo-FISH for LacO, Chr7 and ChrX loci was performed according to a described protocol (Takei et al., 2017). To prepare samples, cells were grown in a Ibidi chamber slide with a removable 12 well silicone chamber (Ibidi, Inc), fixed with 4% PFA for 20 min, washed with PBS twice, and permeabilized in 70% ethanol at −20°C overnight. After that, the samples were treated with methanol/acetic acid (4:1, prechilled at −20°C) at room temperature for 1 hr, washed with PBS twice, treated with 0.1mg/ml RNase A in PBS at 37°C for 1 hr, washed again with PBS twice, and dehydrated by consecutive incubations in 70%, 85% and 100% ethanol. After air-drying, samples were heated at 95°C for 10min in 70% denaturing buffer (2*SSC, 70% formamide) and washed with 2*SSC. For oligo-FISH, hybridization was performed with 10nM-200nM fluorescent nucleotide probes in hybridization buffer (2*SSC, 50% formamide, 10% Dextran Sulfate) at 37°C overnight. After hybridization, samples were washed three times in 50% wash buffer (2*SSC, 50% formamide, 0.1% Triton X-100) and then washed once with 2*SSC. After removing the silicone chamber and drying the slide, the samples were treated with Prolong Diamond Antifade Mountant with DAPI (ThermoFisher, P36966) and covered with cover glasses for imaging. Commercial FISH probes were hybridized according to the manufacturer's protocols.

Immunostaining of nuclear body markers

To detect co-localization of Cajal bodies and targeted LacO loci, U2OS 2-6-3 cells expressing a low level of PYL1-sfGFP-Coilin were transfected with lentivirus encoding PGK-ABI-dCas9-P2A-Puro and sgLacO on day 0, treated with puromycin and 3mM ABA on day 1, and fixed on day 2 after 20 hr of ABA treatment. We performed FISH to detect LacO loci by using Alexa Fluor 647 labeled FISH probes in fixed cells. Immunohistochemistry was performed by using mouse monoclonal anti-SMN (Santa Cruz, Cat.# sc-32313), anti-Fibrillarin (Abcam, Cat.# ab4566), anti-Gemin2 antibody (Santa Cruz, Cat.# sc-32806), and a donkey anti-mouse Alex Fluor 594 secondary antibody (ThermoFisher, Cat.# A-21203).

To detect co-localization between PML body markers and targeted Chr3 loci, U2OS cells expressing PYL1-sfGFP-PML and PGK-ABI-dCas9 were transfected with lentivirus coding dCas9-HaloTag (for CRISPR imaging) and sgChr3 on day 0, treated with puromycin and 3mM ABA on day 1, stained by JF549-HaloTag and fixed in 4% paraformaldehyde (PFA) on Day 3. Immunostaining was performed in fixed samples with rabbit polyclonal anti-SP100 (Abcam, Cat.# ab43151), and donkey anti-rabbit Alex Fluor 647 secondary antibody (ThermoFisher, Cat.# A-31573).

For immunostaining, fixed samples were permeabilized in permeabilization buffer (PBS, 1%Triton X-100) for 15 min, blocked in blocking buffer (PBS, 0.3%Triton X-100, 5% Donkey normal Serum) for 1h, and incubated with primary antibody overnight at 4°C. On the second day, samples were washed in PBS three times, then incubated with the secondary antibody at room temperature for 1-2 hr, and washed four times in PBS before imaging.

Chemical induction and reversal experiment

For targeting genomic loci to nuclear compartments, U2OS cells containing chemical-inducible CRISPR-GO systems and sgRNAs are treated with abscisic acid (ABA, Sigma-Aldrich, A1049) at 3mM for 2 days before imaging or fixation.

For the time-course chemical induction experiment targeting Chr3 to the nuclear periphery, U2OS cells containing CRISPR-GO, CRISPR imaging system, and the sgRNA targeting Chr3 were treated with or without 3mM ABA, stained by JF549-HaloTag, and fixed at different time points. For the time-course chemical reversal experiment, the Chr3-targeting CRISPR-GO cells were pre-treated with 3mM ABA for 2 days, washed five times, and switched to medium without ABA. Cells were stained by JF549-HaloTag ligand for CRISPR imaging and fixed in 4% paraformaldehyde for 20 min at different time points. A sample with no ABA treatment was imaged at the same time as a control.

For the time-course chemical induction experiment targeting LacO to Cajal body, U2OS 2-6-3 cells expressing a low level of PYL1-sfGFP-Coilin were transfected with lentivirus coding PGK-ABI-BFP-dCas9 and sgLacO on day 0, treated with puromycin on day 1, treated with 3mM ABA on day 2, and fixed after 30 min of ABA treatments. For the time-course reversal experiment, cells were pre-treated with 3mM ABA for 1 day, washed five times, and switched to medium without ABA. Cells were fixed in 4% paraformaldehyde for 20 min at different time points.

Cell cycle synchronization

To investigate the mitosis-dependent effect of genomic re-positioning to the nuclear periphery, U2OS cells containing CRISPR-GO and CRISPR imaging systems and the sgRNA targeting Chr3 were used for this experiment. On day −3, cells were starved in 0.5% FBS in DMEM medium for 2 days. On day −1, cells were switched to normal growth medium with 10% FBS and treated with 2mM hydroxyurea (HU) for G1/S phase blockage. On day 0, while keeping the HU treatment, cells were treated with or without ABA. Control cells were treated in the same way but without HU. Cells were stained by JF549-HaloTag for CRISPR imaging and fixed in 4% paraformaldehyde 24h and 48h after ABA treatment.

Microscopy and real-time imaging

With the exception of Figure 2C, all microscopy was performed on a Nikon TiE inverted confocal microscope equipped with an Andor iXon Ultra-897 EM-CCD camera and 405nm, 488nm, 561nm and 642nm lasers, using the 100 × PLAN APO oil objective (NA = 1.49), the 60 × PLAN APO oil objective (NA = 1.40) or the 60 × PLAN APO IR water objective (NA = 1.27). Images were taken using NIS Elements version 4.60 software by time-lapse microscopy with Z stacks at 0.2μm or 0.4μm steps. For live cell imaging, cells were kept at 37°C and 5% CO_2 in a humidified chamber.

For long-term live cell imaging shown in Figure 2C, microscopy was performed in Leica DMi8 inverted microscope equipped with the 63 × HC PLAN APO oil objective (NA = 1.40), a Leica DFC9000 CT camera and a Lumoncor SOLA SM II 405 light source. Images were taken using LAS X Software by time-lapse microscopy every 30 min for 20 hr, using GFP and TXR filter cubes. During imaging, cells were kept at 37°C and 5% CO_2 in a humidified chamber (Okolab Cage incubation system).

To visualize the dynamics of chromatin-Cajal body interactions in individual cells (Figure 4), U2OS 2-6-3 cells expressing a lower level of PYL1-sfGFP-Coilin was transfected with lentivirus coding PGK-ABI-BFP-dCas9 and sgLacO on day 0, treated with puromycin on day 1 and seeded on Ibidi 96 well μ-plates (Ibidi. Inc). Confocal microscopy was used to image each well by focusing on a ABI-BFP-dCas9 labeled LacO locus within a chosen cell. Images were captured before ABA treatment for comparison. Without moving the sample under the confocal microscope, 10-fold ABA-containing culture medium was added to the imaging well to reach a final concentration of 1mM ABA. The same cell containing the previously focused LacO locus was immediately imaged after adding ABA. Immediately after ABA addition, the first image taken was assigned as t = 0, and all other images were aligned in time accordingly.

Image processing and analysis

Image processing was performed by Fiji (ImageJ) (Schindelin et al., 2012) or MetaMorph (Molecular devices, CA). A single microscope plane showing maximum fluorescence of labeled genomic loci, or the average of two/three adjacent Z planes showing maximum loci fluorescence is shown in figures. Some images were processed using the "smooth" function in Fiji to reduce noises for visualization purposes only.

Line scan was performed using the "Analyze/Plot Profile" function in Fiji, analyzed in Excel and plotted in GraphPad Prism (Version 7.00 for Mac OS, GraphPad Software, La Jolla California USA, https://www.graphpad.com). Fluorescence intensity at each point along the line was normalized relative to the maximum (= 1) and the minimum (= 0) fluorescence intensity along the line.

We used Imaris software (Bitplane, inc) to perform 3D visualization and reconstitution of representative cells targeting telomeres to the nuclear envelope (Videos S1&S2). Telomere spots were built using the Spots function, and the surface of the nuclear periphery was built as a membrane object using the Cell function and then switched to a surface object. The distance between telomeres and the nuclear envelope was quantified by using the reconstituted telomere spots and the nuclear periphery surface.

Flow cytometry fluorescence assays

For quantification of CFP-SKL expression adjacent to LacO loci, U2OS 2-6-3 cells containing ABI-dCas9-P2A-mCherry and PYL1-sfGFP-Emerin or PYL1-sfGFP-Coilin were transduced with rtTA (reverse tetracycline-controlled transactivator) and sgRNA targeting lacO loci or non-targeting sgRNAs, treated with ABA at 3mM for 2 days and then induced with doxycycline at 50ng/ml for 40 hr (nuclear periphery tethering) or 24 hr (Cajal body tethering). After treatment, U2OS 2-6-3 cells were dissociated using 0.25% Trypsin EDTA (Life Technologies) and analyzed by flow cytometry on CytoFlex S (Beckman Coulter Life Sciences) using 405nm, 488nm and 561 lasers. At least 8,000 cells were analyzed for each sample. Cells were gated for positive dCas9 (mCherry) and Emerin/Coilin (GFP) expression. CFP-SKL fluorescence was detected using the 405nm laser and the 450/45 filter. To quantify relative fluorescence, the average total fluorescence of untreated cells (without Dox and ABA) was set to 0, while the average total fluorescence of doxycycline induced cells (with Dox only) was set to 1. Technical duplicates of 3 experimental replicates were analyzed. The number of technical replicates is shown as individual dots in Figure 5 and Figure S4.

qRT-PCR

Real-time qRT-PCR was performed to determine the expression change of endogenous genes. For each sample, total RNA was isolated by using the RNeasy Plus Mini Kit (QIAGEN Cat 74134), followed by cDNA synthesis using the iScript cDNA Synthesis Kit (BioRad, Cat 1708890). Quantitative PCR was performed using the PrimePCR assay with the SYBR Green Master Mix (BioRad), and run on a Biorad CFX384 real-time system (C1000 Touch Thermal Cycler), according to manufacturers' instructions. Cq values were used to quantify gene expression. The relative expression of the *PPP1R2* and *ACAP2* genes was normalized to a *GAPDH* internal control. To calculate the relative mRNA expression level, the relative expression of each treatment was normalized by setting the average value in non-ABA treated samples as 1. Technical duplicates in 3 experimental replicates were analyzed. The number of technical replicates is shown as individual dots in Figure 5C and Figure S4B, D.

Cell viability assay

A cell viability assay was performed by using Alamarblue cell viability reagents (ThermoFisher Scientific), which quantifies cell proliferation rate by measuring the metabolic activity of the cells. For each condition, 100μl of cells treated with and without ABA were seeded at equal concentration (500-1000 cells/well) in the same 96-well plate. At the time of detection, 10μl of Alamarblue reagents were added to each well and the plates were incubated at 37°C for 1 hr. After that, the fluorescent intensity was measured in the Synergy H1 microplate reader (Biotek) using an excitation wavelength of 540nm and emission wavelength of 585nm. Average fluorescent intensity of wells containing only 100μl culture medium (-/+ ABA) was used as blanks. For each well, the relative fluorescent intensity was calculated by subtracting background (average intensity of blank wells) from raw fluorescent intensity values. To

calculate the relative cell viability, the relative florescent intensity in each well was normalized by setting the average value in non-ABA treated wells as 1. Technical duplicates in 3 experimental replicates were analyzed. The number of technical replicates is shown in the figures as individual dots.

Cell cycle cytometry analysis

To quantify how telomere nuclear periphery tethering affects cell cycle progression, U2OS cells containing the nuclear periphery tethering system were treated with lentiviruses coding sgTelomere and TRF1-mcherry, or non-targeting control sgRNA. Telomere tethering was confirmed by microscopy after 2 days of ABA treatment. After 3 day of ABA treatment, control and treated cells were dissociated using 0.25% Trypsin EDTA, stained with Hoechst 33342 at 1:1000 dilution for 1h, and analyzed by flow cytometry on CytoFlex S (Beckman Coulter Life Sciences) using 405nm lasers. At least 20,000 cells were analyzed for each sample. Cell cycle analysis was performed using FlowJo (FlowJo, LLC).

Identification of repetitive sequences

We used Tandem Repeats Finder software (Benson, 1999) to identify all tandem repeats of 14-nucleotides or longer sequences from the human genome (hg38). Regions that contains ten or more identical tandem repeats were defined a "repetitive sequence cluster." We mapped these repetitive sequence clusters to each human chromosome. Distances between the repetitive sequence clusters and genes were calculated using the BEDTools suite.

QUANTIFICATION AND STATISTICAL ANALYSIS

Quantification of genomic repositioning

To determine the peripheral recruitment efficacy in living U2OS cells, Chr3, Chr13 and LacO (Chr1) loci were labeled by CRISPR-Cas9 imaging and telomeres were labeled by TRF1-mCherry, while the nuclear envelope was labeled by PYL1-sfGFP-Emerin. After scanning Z stacks of confocal planes, the position of each labeled locus was viewed in slice viewer (NIS element viewer) to determine its position in XY, XZ and YZ planes. Loci were calculated only once and then categorized into three categories: (1) loci locate directly in the nuclear periphery that colocalize with PYL1-GFP-Emerin in XY, YZ and YZ planes, (2) loci that do not co-localize with PYL1-GFP-Emerin, and (3) loci that colocalize with internal PYL1-GFP-Emerin not at nuclear periphery (in rare cases). The number of loci in each category was recorded for each individual cell. Only loci of the first category that colocalized with PYL1-GFP-Emerin at the nuclear envelope were counted as nuclear periphery positioned loci. Cells containing at least one nuclear periphery positioned loci were quantified.

To determine peripheral recruitment efficacy in fixed U2OS cells (e.g., Chr7, ChrX, *PTEN*, *CXCR4*, *XIST*), targeted genomic loci were labeled by FISH and the nuclei were stained by DAPI. After scanning Z stacks of confocal planes, the position of each labeled locus was viewed in 3D space to determine its position in XY, XZ and YZ planes. A genomic locus that located at the edge of the nucleus (DAPI) in 3D space was categorized as a periphery-located locus. Otherwise it was considered as an internal-located locus. The number of loci in each category was recorded for each individual cell. Cells containing at least one nuclear periphery positioned loci were also quantified.

To determine the Cajal body co-localizing efficacy in fixed U2OS 2-6-3 cells, targeted LacO loci were labeled by FISH, nuclei were stained by DAPI, and Cajal bodies (CBs) were labeled by PYL1-GFP-Coilin. After scanning Z stacks of confocal planes, we identified the position of each LacO locus in 3D space. Without double counting, the loci were categorized into two categories: loci that co-localize with CBs, and loci that do not co-localize with CBs. The number of loci in each category was recorded for each individual cell. Cells containing at least one CB-colocalized loci were also quantified.

To determine the co-localizing efficacy between endogenous Chr3 loci and nuclear bodies (CBs and PML bodies), targeted Chr3 loci were labeled by CRISPR-Cas9, and CBs were labeled by PYL1-GFP-Coilin, or PML bodies were labeled by PYL1-GFP-PML. After scanning Z stacks of confocal planes, we identified the position of each Chr3 locus in 3D space. Without double counting, the loci were categorized two categories: loci that colocalize with nuclear bodies (CBs or PML bodies), and loci that do not colocalize with nuclear bodies (CBs or PML bodies). The number of loci in each category was recorded for each individual cell. Cells containing at least one nuclear body-colocalized loci were also quantified.

Short-term genomic tracking

Genomic loci were tracked by using the TrackMate plugin (Tinevez et al., 2017) in Fiji. For tracking genomic loci, the estimated blob diameter was set between 0.5-1 μm. Linking max distance was set to 2 μm, gap closing distance was set to 3 μm, and gap closing max frame was set to 2. Position of each locus(x^t, y^t) at different time points (*t*) were measured, analyzed in Excel and plotted in GraphPad Prism 7. The movement step (*d*x, *d*y) was calculated by subtracting the position of a previous time point from the new position: $dx^t = x^t - x^{t-1}$&$dy^t = y^t - y^{t-1}$, where(x^t, y^t) was the position of a locus at time *t*, and (x^{t-1}, y^{t-1}) was the position of the locus at the previous time point (*t-1*). Step distance = $\sqrt{(x^t - x^{t-1})^2 + (y^t - y^{t-1})^2}$ was calculated by how far a locus moved away from its position at the previous time point.

To compare step distances, 1696 step distances of 19 interior-localized Chr3 loci and 1669 step distances of 14 peripherally localized Chr3 loci were analyzed. The two-side t test with unequal variance was performed.

Statistical Analysis

For quantification of re-localization efficacy (Figures 1C–1F, Figures 2A–2B, Figures 3C, 3F, &3I, Figures 4A–4B and Figure S3D), *p* values were calculated using Fisher's exact test in GraphPad, and error bars show standard error of the mean (SEMs) calculated according to Bernoulli distributions. The number of counted loci and cells are listed at the bottom of each figure. For Figure 2F, Figures 5A–5C, Figure 5E, Figure S4 and Figures S5C and S5D, the *p* values were calculated using two-sided t test with unequal variance in Excel and error bars showing standard deviations. Technical duplicates in 3 experimental replicates were analyzed. The number of technical duplicates are shown in figures as individual dots. For Figures 2F–2G, step distances of untethered (1696 steps of 19 loci) and tethered (1669 steps of 14 loci) Chr3 loci were analyzed. For Figure 2G, we fit Gamma distributions by maximum likelihood by using the R package fitdistrplus and used the Kolmogorov-Smirnov test for validation ($p = 0.06$ for periphery loci & $p = 0.77$ for interior loci). Fitted parameters: shape parameter $k = 2.4$ for untethered loci and 1.9 for tethered loci; rate parameter $\beta = 21.9$ for untethered loci and 46.3 for tethered loci.

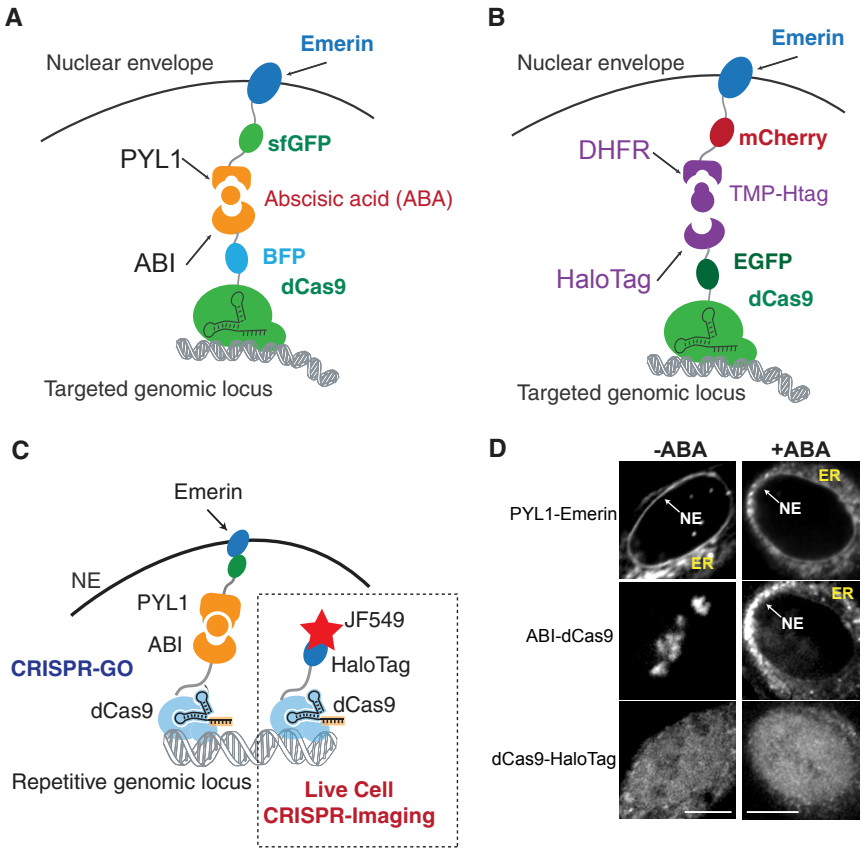

Figure S1. Schematics of Two Chemically Inducible CRISPR-GO Systems and CRISPR-Cas9 Imaging, Related to Figure 1

(A) Schematic of an abscisic acid (ABA)-inducible CRISPR-GO system for targeting genomic loci to the nuclear periphery through co-expression of ABI-BFP-dCas9 and PYL1-GFP-Emerin. ABI and PYL1 dimerize in the presence of ABA and causes relocalization of the ABI-dCas9-targeted genomic loci to PYL1-GFP-Emerin at the nuclear periphery.

(B) Schematic of a Trimethoprim-Haloligand (TMP-HTag)-inducible CRISPR-GO system for targeting genomic loci to the nuclear periphery through co-expression of dCas9-EGFP-HaloTag and DHFR-Emerin-mCherry in human cells. TMP-HTag treatment dimerizes DHFR and HaloTag to potentially re-localize dCas9-EGFP-HaloTag-targeted genomic loci to the nuclear periphery containing DHFR-Emerin-mCherry.

(C) Schematic of the CRISPR-Cas9 imaging method used to visualize repetitive genomic loci targeted by the CRISPR-GO system in living cells. By using the same sgRNA to target multiple repeats, both AB1-dCas9 and dCas9-HaloTag binds to the same repetitive genomic locus. While AB1-dCas9 dimerizes with PYL1-Emerin to re-localize the genomic locus, dCas9-HaloTag binds to a cell-permeable JF549-HaloTag dye ligand to enable visualization of the targeted genomic locus in living cells.

(D) Representative microscopic images of U2OS cells showing co-expression of AB1-BFP-dCas9, PYL1-GFP-Emerin, and dCas9-HaloTag, without sgRNAs. In the absence of ABA, AB1-BFP-dCas9 usually accumulated within nucleoli, while PYL-GFP-Emerin located at the nuclear envelope (NE) and endoplasmic reticulum (ER). ABA-induced heterodimerization relocated AB1-BFP-dCas9 to the NE and ER, as marked by PYL1-GFP-Emerin. dCas9-HaloTag had a low expression level and was evenly distributed throughout the nucleus; its location remained unaffected by ABA treatment. Scale bars, 10μm.

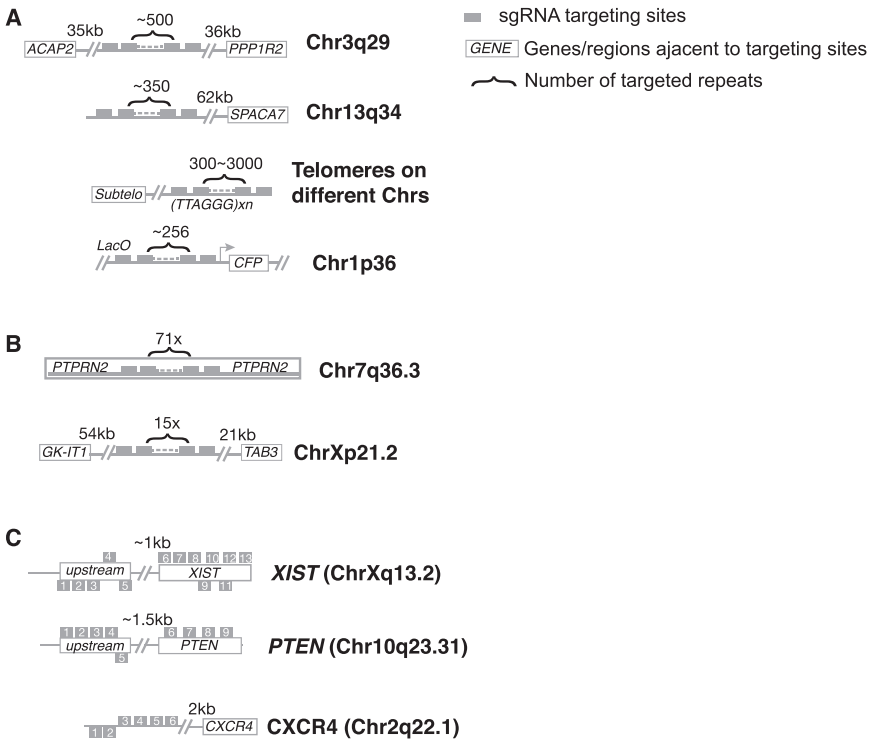

Figure S2. A Summary of Genomic Loci Used for CRISPR-GO Repositioning in This Study, Related to Figure 1

(A and B) Summary of chromosome locations of highly repetitive (A) and less repetitive (B) regions targeted by CRISPR-GO in Figures 1C–1D. A single sgRNA binds to multiple repeats (solid gray boxes) within the targeted regions. The genes/regions adjacent to the targeted site are shown in italic letters in gray-outlined boxes. See also Table S1.

(C) Chromosome location of non-repetitive regions targeted by CRISPR-GO in Figures 1E–1F. Multiple sgRNAs were designed to tile along the regions upstream or within the gene bodies of the targeted genes (*XIST*, *PTEN*, *CXCR4*). The sgRNA-targeted regions are shown in solid gray boxes. The top gray boxes show sgRNA targets within the forward strand and bottom gray boxes show sgRNA targets within the reverse strand. The genes/regions adjacent to the targeted site are shown in italic letters in gray boxes. See also Table S2.

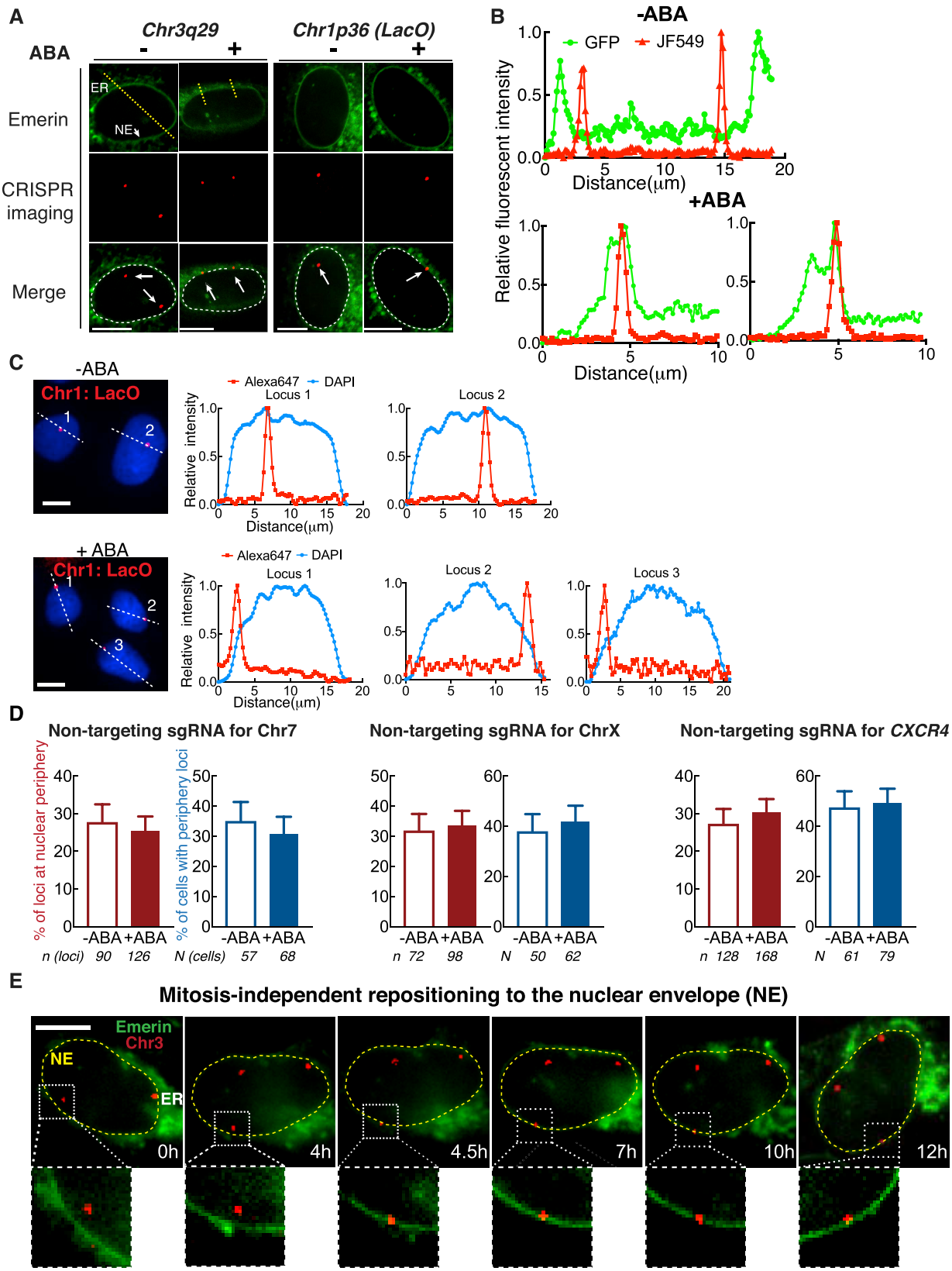

(legend on next page)

Figure S3. Re-localization of Genomic Loci to Nuclear Periphery by the CRISPR-GO System, Related to Figures 1 and 2

(A) Individual channels of representative microscopic images in Figure 1G comparing the localization of targeted genomic loci (red, arrows) and nuclear periphery (green, dotted lines) with or without ABA. The top row shows PYL1-GFP-Emerin (green) that is localized to the nuclear envelope (NE) and endoplasmic reticulum (ER). The nuclear periphery is outlined by dotted white lines (bottom) except for regions next to tethered genomic loci. Scale bars, 10μm.

(B) Linescans of the relative fluorescence intensity of labeled Chr3 loci (red) and PYL1-GFP-Emerin (green) without (top) and with ABA treatment (bottom) along the yellow dotted lines as shown in (A). Chr3 loci are labeled by CRISPR-Cas9 imaging (dCas9-HaloTag) through the addition of the JF549-HaloTag dye.

(C) CRISPR-GO mediated repositioning of LacO Loci to the nuclear periphery. Left: representative microscopic images of labeled LacO loci (red, by FISH, Alexa Fluor 647) and the nucleus (blue, DAPI) without (top) and with ABA treatment (bottom). Right: linescan of the relative fluorescence intensity of LacO loci (red, Alexa Fluor 647) and the nucleus (blue, DAPI) along the dotted lines as shown in left. Scale bars, 10μm.

(D) Quantification of percentages of nuclear periphery localized genomic loci (Chr7, ChrX, and *CXCR4*) in CRISPR-GO cells transfected with a non-targeting sgRNA in -/+ABA conditions. Red: percentage of genomic loci at the nuclear periphery, n = total loci analyzed; Blue: percentage of cells containing at least one nuclear-periphery-localized locus, N = total cells analyzed. Data are represented as mean ± SEM.

(E) Representative microscopic images showing mitosis-independent tethering of endogenous genomic loci to the nuclear periphery. The insets are also shown in Figure 2C. Green shows PYL1-GFP-Emerin that is localized to the nuclear envelope (NE) and the endoplasmic reticulum (ER). The nuclear envelope is outlined by dotted yellow lines. The Chr3 locus (in red) is not adjacent to the nuclear envelope during the first 4h of recording. Localization to the nuclear periphery occurs at 4.5h and remains tethered for the rest of the 8 h of recording. Nuclear rotation happens between 10h and 12h. Scale bar, 10μm.

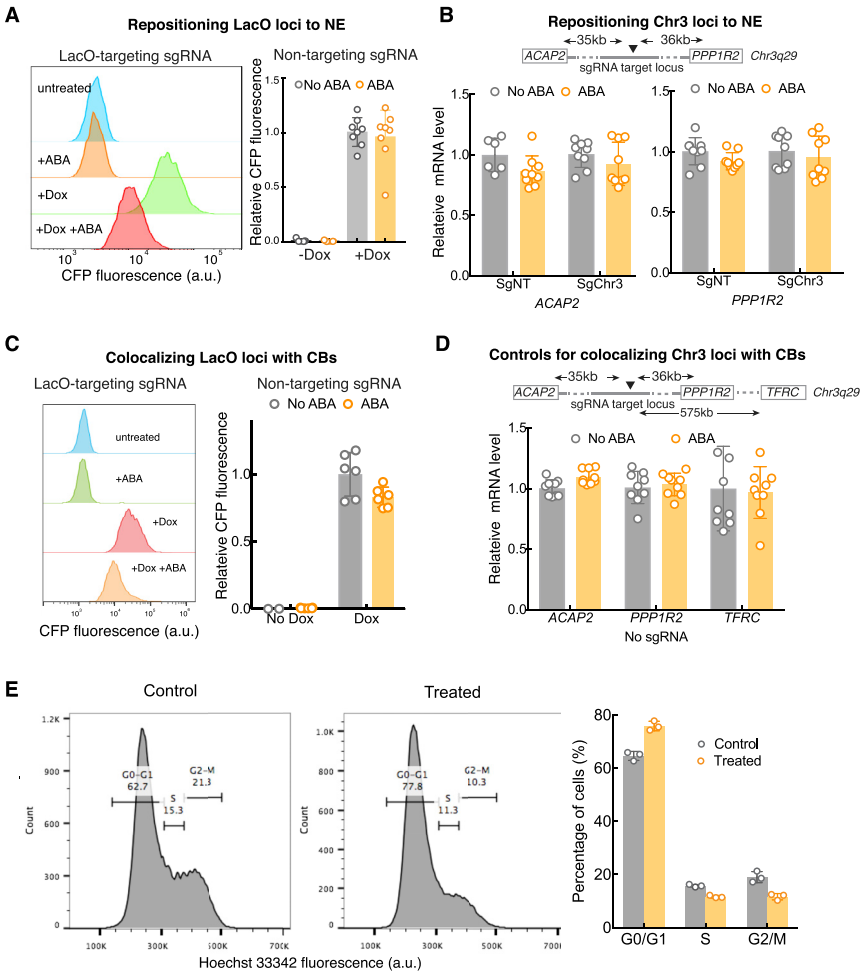

Figure S4. Effects of CRISPR-GO on Gene Expression and Cellular Phenotypes, Related to Figure 5

(A) Representative flow cytometry histograms (Left) comparing the fluorescence intensity of the CFP reporter using CRISPR-GO to tether LacO loci to the nuclear periphery in ± Dox and ± ABA conditions. The statistics diagram is shown in Figure 5A. The right diagram shows quantification of the relative CFP fluorescence with a non-targeting sgRNA in ± Dox and ± ABA conditions. Data are represented as mean ± SD.

(B) Comparison of *ACAP2* and *PPP1R2* gene expression when using the CRISPR-GO system to reposition Chr3 loci to the nuclear periphery. mRNA was measured using qRT-PCR under different conditions. Cells were transfected with a non-targeting sgRNA (sgNT) or a Chr3 targeting sgRNA (sgChr3). Data are represented as mean ± SD.

(C) Representative flow cytometry histograms (left) comparing the fluorescence intensity of CFP reporter expression using CRISPR-GO tethering LacO loci to CBs in ± Dox and ± ABA conditions. The statistics diagram is shown in Figure 5B. The right diagram shows the quantification of relative CFP fluorescence with a non-targeting sgRNA in ± Dox and ± ABA conditions. With a non-targeting sgRNA, ABA treatment leads to a slight but insignificant decrease ($p > 0.05$) in CFP reporter expression. Data are represented as mean ± SD.

(D) Controls for using CRISPR-GO to colocalize the endogenous Chr3 loci with CBs. Measurement of *ACAP2*, *PPP1R2* and *TFRC* mRNA expression with the CRISPR-GO system, but without a targeting sgRNA in ± ABA conditions. See Figure 5C for expression data with a Chr3 targeting sgRNA. mRNA was measured using qRT-PCR under different conditions. Data are represented as mean ± SD.

(E) Cell cycle analysis of cells when CRISPR-GO was used to reposition telomeres to the nuclear periphery. Cells were treated with ABA for 3 days. Left: representative flow cytometry histograms compare the fluorescence Hoechst 33342 stained DNA components in telomere-targeting sgRNA treated cells and non-targeting sgRNA control cells. Right: quantification of the percentage of cells at G1/G0, S and G/M phase of the cell cycle. Data are represented as mean ± SD.

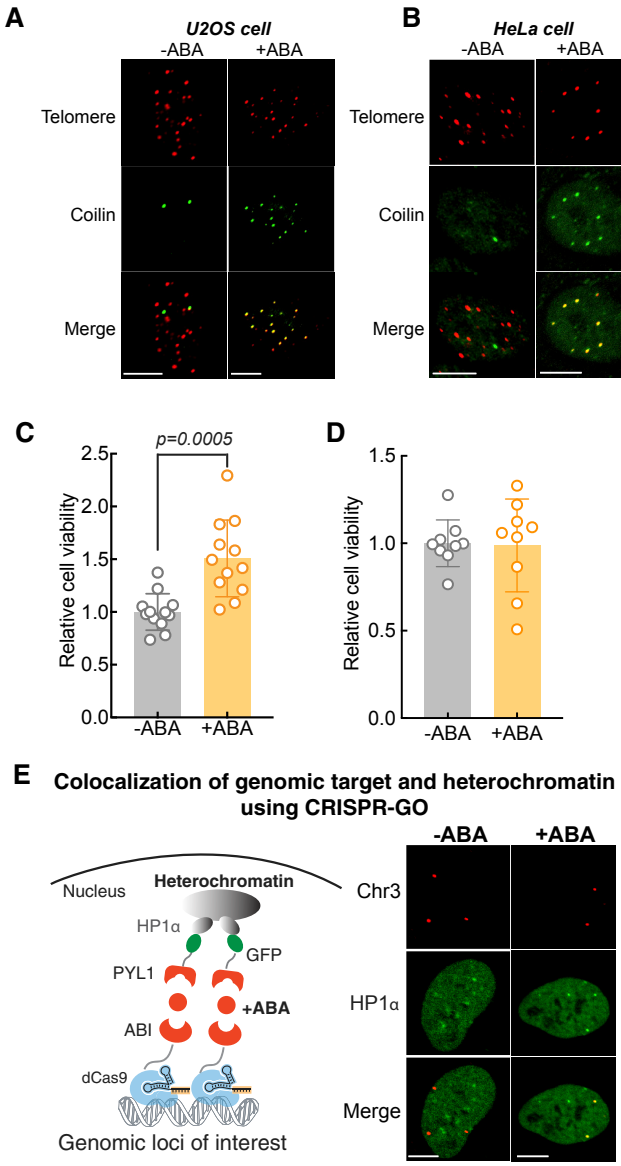

Figure S5. Other CRISPR-GO Applications, Related to Figure 5

(A and B) Representative microscopic images of U2OS cells (A) and HeLa cells (B) using CRISPR-GO system to colocalize telomeres (TRF1-mCherry, red, top) with CBs (GFP-Coilin, green, middle) in ± ABA conditions. Scale bars, 10μm.

(C) Comparison of relative U2OS cell viability using the CRISPR-GO system targeting telomeres to CBs with or without ABA. Cells were treated with ABA for two days. Cell viability was measured by an Alamar blue assay. Data are represented as mean ± SD.

(D) Comparison of relative cell viability of U2OS cells with or without ABA. Cells were treated with ABA for two days. Cell viability was measured by an Alamar blue assay. Data are represented as mean ± SD.

(E) Schematic of an ABA-inducible CRISPR-GO system (left) for targeting genomic loci to heterochromatin through co-expression of ABI-dCas9 and PYL1-GFP-HP1α in human cells. Representative microscopic images (right) of ABI-dCas9-targeted Chr3 loci colocalized with PYL1-GFP-HP1α after ABA treatment. Scale bars, 10μm.

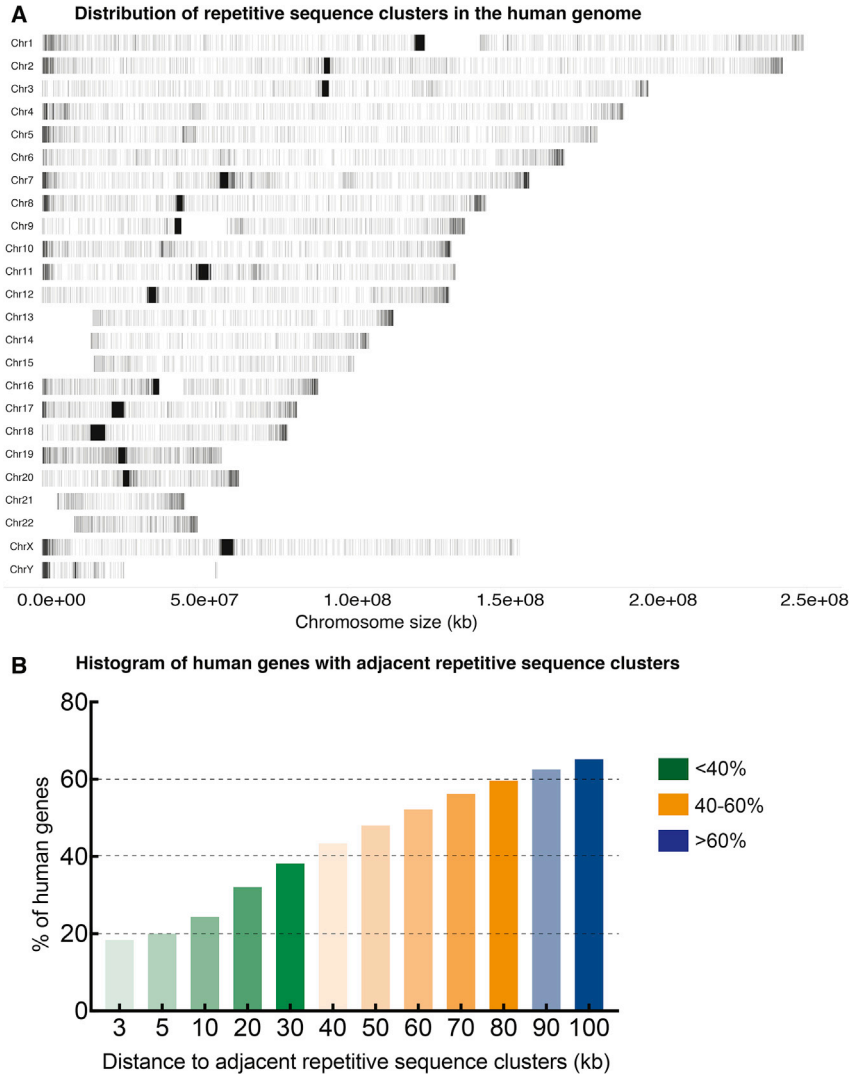

Figure S6. Distribution of Repetitive Sequences in the Human Genome and Adjacent Genes, Related to Figure 6

(A) The distribution of repetitive sequences (four or more) for each human chromosome and their relative coordinates.

(B) Genome-wide bioinformatics analysis reveals the percentage of human genes located within a given distance to adjacent repetitive sequences.